Nuclear GRP75 Binds Retinoic Acid Receptors to Promote Neuronal Differentiation of Neuroblastoma

Yu-Yin Shih[1,2], Hsinyu Lee[2,3], Akira Nakagawara[4], Hseuh-Fen Juan[3,5], Yung-Ming Jeng[6], Yeou-Guang Tsay[7], Dong-Tsamn Lin[8,9], Fon-Jou Hsieh[10], Chien-Yuan Pan[2,3]*, Wen-Ming Hsu[9,11]*, Yung-Feng Liao[1]*

1 Laboratory of Molecular Neurobiology, Institute of Cellular and Organismic Biology, Academia Sinica, Taipei, Taiwan, **2** Institutes of Zoology, National Taiwan University, Taipei, Taiwan, **3** Department of Life Science, National Taiwan University, Taipei, Taiwan, **4** Department of Molecular Biology and Oncology, Chiba Cancer Center Research Institute, Chiba University Graduate School of Medicine, Chiba, Japan, **5** Institute of Molecular and Cellular Biology, National Taiwan University, Taipei, Taiwan, **6** Department of Pathology, National Taiwan University Hospital and National Taiwan University College of Medicine, Taipei, Taiwan, **7** Institute of Biochemistry and Molecular Biology and Proteomics Research Center, National Yang-Ming University, Taipei, Taiwan, **8** Department of Pediatrics, National Taiwan University Hospital and National Taiwan University College of Medicine, Taipei, Taiwan, **9** Childhood Cancer Foundation, Taipei, Taiwan, **10** Graduate Institute of Clinical Medicine, National Taiwan University College of Medicine, Taipei, Taiwan, **11** Department of Surgery, National Taiwan University Hospital and National Taiwan University College of Medicine, Taipei, Taiwan

Abstract

Retinoic acid (RA) has been approved for the differentiation therapy of neuroblastoma (NB). Previous work revealed a correlation between glucose-regulated protein 75 (GRP75) and the RA-elicited neuronal differentiation of NB cells. The present study further demonstrated that GRP75 translocates into the nucleus and physically interacts with retinoid receptors (RARα and RXRα) to augment RA-elicited neuronal differentiation. GRP75 was required for RARα/RXRα-mediated transcriptional regulation and was shown to reduce the proteasome-mediated degradation of RARα/RXRαin a RA-dependent manner. More intriguingly, the level of GRP75/RARα/RXRα tripartite complexes was tightly associated with the RA-induced suppression of tumor growth in animals and the histological grade of differentiation in human NB tumors. The formation of GRP75/RARα/RXRα complexes was intimately correlated with a normal MYCN copy number of NB tumors, possibly implicating a favorable prognosis of NB tumors. The present findings reveal a novel function of nucleus-localized GRP75 in actively promoting neuronal differentiation, delineating the mode of action for the differentiation therapy of NB by RA.

Citation: Shih Y-Y, Lee H, Nakagawara A, Juan H-F, Jeng Y-M, et al. (2011) Nuclear GRP75 Binds Retinoic Acid Receptors to Promote Neuronal Differentiation of Neuroblastoma. PLoS ONE 6(10): e26236. doi:10.1371/journal.pone.0026236

Editor: Branden Nelson, Seattle Children's Research Institute, United States of America

Received May 10, 2011; **Accepted** September 22, 2011; **Published** October 14, 2011

Funding: This study was supported by the National Health Research Institutes (NHRI-EX96-9620NI to W.-M.H.), National Science Council, Taiwan (NSC 95-2314-B-002-155-MY2 to W.-M.H.), and Academia Sinica (to Y.-F.L.). The National RNAi Core Facility located at the Institute of Molecular Biology/Genomic Research Center, Academia Sinica, is supported by the National Core Facility Program for Biotechnology Grants of NSC (NSC 100-2319-B-001-002). The funders had no role in study design, data collection and analysis, decision to publish, or preparation of the manuscript.

Competing Interests: The authors have declared that no competing interests exist.

* E-mail: yliao@sinica.edu.tw (YFL); billwmhsu@gmail.com (WMH); cypan@ccms.ntu.edu.tw (CYP)

Introduction

Neuroblastoma (NB) is the most common and deadly cancer in patients who are identified during the first year of life, and are often diagnosed as an aggressive and metastatic disease that leads to high mortality [1]. Despite the noted improvement in the overall outcome in patients with NB, the 5-year survival rates among children with high-risk NB have only improved slightly. This result is mainly attributed to the fact that key molecular pathways controlling NB tumorigenesis remain elusive.

Current treatments for NB include a combination of chemotherapy, surgery, radiation, bone marrow transplantation, immunotherapy, and differentiating agents [2]. NB is the only pediatric cancer treated with differentiation reagents as the first-line of defense [2]. One of the most potent differentiation inducers for NB is retinoic acid (RA) [3,4]. The results of independent trials have consistently shown that the administration of RA significantly improves the overall survival rates after bone-marrow transplantation [5,6,7]. Consistent with these findings, NB cells treated with all-trans RA at doses used clinically display evident neuronal differentiation and reduced proliferation [8]. Therefore, the elucidation of molecular mechanisms underlying RA-induced neuronal differentiation in NB could pave the way for the development of novel therapeutic strategies for NB.

RA-elicited signaling is primarily mediated by retinoid receptors [9]. The retinoid receptors can be categorized into two subfamilies: retinoic acid receptors (RARs) and retinoid X receptors (RXRs). Upon binding RA, the ligand-bound RAR/RXR heterodimers undergo a conformational change, causing their translocation to the nucleus, where they act as transcription factors targeting retinoic acid responsive elements (RARE) within the promoters of genes involved in differentiation and growth arrest [10,11]. Recent studies show that the activity of RA receptors can be regulated by posttranslational modifications, such as phosphorylation and ubiquitination [12]. Moreover, the ligand-induced transactivation of RAR/RXR heterodimers could also be modulated by various adaptor proteins in the nucleus [13].

Glucose-regulated protein 75 (GRP75) was first identified as a member of the Hsp70 family that could function in multiple subcellular compartments [14]. Accumulated evidence has

demonstrated the versatility of GRP75 in regulating cellular stress responses, mitochondrial homeostasis, intracellular trafficking, antigen presenting, cell proliferation, differentiation, and tumorigenesis [15]. Previous work from our group demonstrated that GRP75 is upregulated in RA-treated NB cells and in NB patients with favorable prognostic outcome [16]. The present study further investigates the possible role of altered GRP75 expression in the regulation of RA-elicited neuronal differentiation in NB.

Results

Nuclear translocation of GRP75 is significantly enhanced upon retinoic acid-induced neuronal differentiation in neuroblastoma cells

We previously demonstrated that GRP75 expression is significantly increased in retinoic acid-treated NB cells and is associated with a favorable prognosis in NB patients [16]. In the present study, immunofluorescence confocal microscopy revealed that GRP75 was highly enriched in the nuclei of RA-treated NB cells compared to untreated cells. The cross-sectional views of stacked images unambiguously revealed that the nuclear translocation of GRP75 was significantly enhanced for an approximately 4-fold increase in RA-treated cells compared to DMSO-treated controls (Figure S1A-C). To further confirm the RA-induced nuclear localization of GRP75, the levels of GRP75 in both nuclear and cytoplasmic fractions prepared from RA- and DMSO-treated NB cells were determined by Western blotting, and the results showed a dramatic increase in nuclear GRP75 in RA-treated cells compared to control cells, while the cytosolic pools of GRP75 remained unchanged in response to RA treatment (Figure S1D). We also found that RA can induce the nuclear translocation of GRP75 in a dose-dependent manner (Figure S13). This RA-induced nuclear translocation of GRP75 was independently confirmed in two separate NB cell lines (SK-N-DZ and SK-N-SH NB, Figure S12). Together, the present findings provide the first direct evidence that GRP75 can be localized to the nucleus, where it potentially plays a critical role in the RA-elicited neuronal differentiation of NB cells.

The interaction between nuclear GRP75 with retinoic acid receptors is significantly enhanced in differentiated NB cells

RA primarily binds to RARα/RXRα heterodimers to transduce its downstream signaling [17]. It is therefore possible that the nucleus-localized GRP75 could be actively involved in the RA-induced neuronal differentiation of NB cells by interacting with RA receptors and modulating their activities. To investigate this possible mechanism, the potential association between GRP75 and RARα/RXRα in the nucleus in response to RA-induced neuronal differentiation was investigated. Using co-immunoprecipitation, a physical interaction between endogenous GRP75 and RARα and RXRα in the nucleus was demonstrated. This novel interaction between GRP75 and RARα/RXRα was significantly enhanced in the nucleus in RA-treated NB cells compared to controls, but it was trivial and irresponsive to RA treatment in the cytosol (Figure 1A, B). Co-immunoprecipitation with a non-specific mouse IgG did not reveal any detectable interaction between GRP75 and RA receptors (Figure S11). Moreover, the co-localization of GRP75 with RARα/RXRα heterodimers was vividly observed in the nucleus of RA-treated SH-SY5Y cells and increased upon RA stimulation (Figure 1C-F, Figure S2), suggesting that RA could selectively and significantly enhance the binding of GRP75 to RARα/RXRα. The interaction between GRP75 and RARα/RXRα was independently validated in two *MYCN*-nonamplified (SK-N-SH and SK-N-MC) and three *MYCN*-amplified NB cell lines (SK-N-DZ, SK-N-BE, and IMR-32) (Figure S3), suggesting a critical role of GRP75 in RA signaling and NB differentiation. Together, these results strongly suggest that GRP75 participates in RA-elicited neuronal differentiation of NB cells through its direct interaction with nuclear RARα/RXRα heterodimers.

Down-regulation of GRP75 inhibits RA-elicited activation of RARα/RXRα receptors

To determine whether the binding of GRP75 to the RARα/RXRα receptor complex in the nucleus is necessary for the RA-induced neuronal differentiation of NB cells, the expression of RA target genes was examined in GRP75-deficient SH-SY5Y cells in the presence or absence of RA. Using an RARα/RXRα-driven luciferase reporter gene construct (RARE-Luc), RA-induced reporter gene expression was determined to be abrogated by the down-regulation of GRP75, suggesting that GRP75 is required for RA-triggered transcriptional regulation (Figure 2A). This finding was further corroborated by data showing that GRP75-deficient SH-SY5Y cells exhibit a significant reduction in the RA-elicited activation of the *RARβ* promoter, a known RARα/RXRα downstream target gene [18] (Figure 2B). The knockdown efficiency of both GRP75-targeting shRNAs was approximately 75%, as seen in the mRNA transcript and protein levels (Figure 2E and Figure S4). Using reporter gene constructs derived from MYCN and NEDD9 promoters [19,20], the depletion of GRP75 in SH-SY5Y cells was further demonstrated to effectively inhibit the RA-elicited stimulation of NEDD9 promoter activity (a neuronal differentiation marker) and abolish the RA-triggered suppression of MYCN promoter activity (a proliferation marker) (Figures 2C, D). The present data clearly suggest that GRP75 could be a novel transcriptional coactivator of RARα/RXRα and therefore modulate RA-elicited neuronal differentiation of NB cells.

To further substantiate the role of GRP75 in RARα/RXRα-mediated transcriptional regulation, the mRNA transcript levels of selected RA target genes were examined by real-time quantitative PCR. Several RA target genes, such as CLMN, CRABP2, HOXD10, RARβ, NAV2, NEDD9, RET, TH, and TrkA, have been shown to promote neuronal differentiation, whereas others, including MYCN, Survivin, and p34, function in cell proliferation [19,21,22,23,24]. In the present study, while the expression of nine RA target genes involved in neuronal differentiation was significantly elevated in RA-treated NB cells compared to controls, knockdown of GRP75 dramatically compromised the RA-induced transcriptional up-regulation of these pro-differentiation target genes in NB cells (Figure 2G). Concomitant with defective neuronal differentiation, down-regulation of GRP75 could favor cell growth by diminishing the RA-elicited transcriptional suppression of pro-proliferation target genes (MYCN, Survivin, and p34) (Figure 2F).

Consistent with the essential role of GRP75 in neuronal differentiation, the ectopic expression of GRP75 in SH-SY5Y cells significantly enhanced RA-triggered transactivation of RARα/RXRα (Figure 3A-C). The GRP75-dependent transcriptional regulation of RA target genes was further explored through the ectopic expression of GRP75 in SH-SY5Y cells. Overexpression of GRP75 significantly potentiated the expression of differentiation-promoting genes and suppressed the expression of pro-proliferation genes in NB cells with or without RA (Figure 3E, F). Together, the regulation of RA-elicited neuronal differentiation by GRP75 was independently confirmed in separate albeit related NB cell lines SH-SY5Y and SK-N-SH (Figure 2, Figure 3, Figure

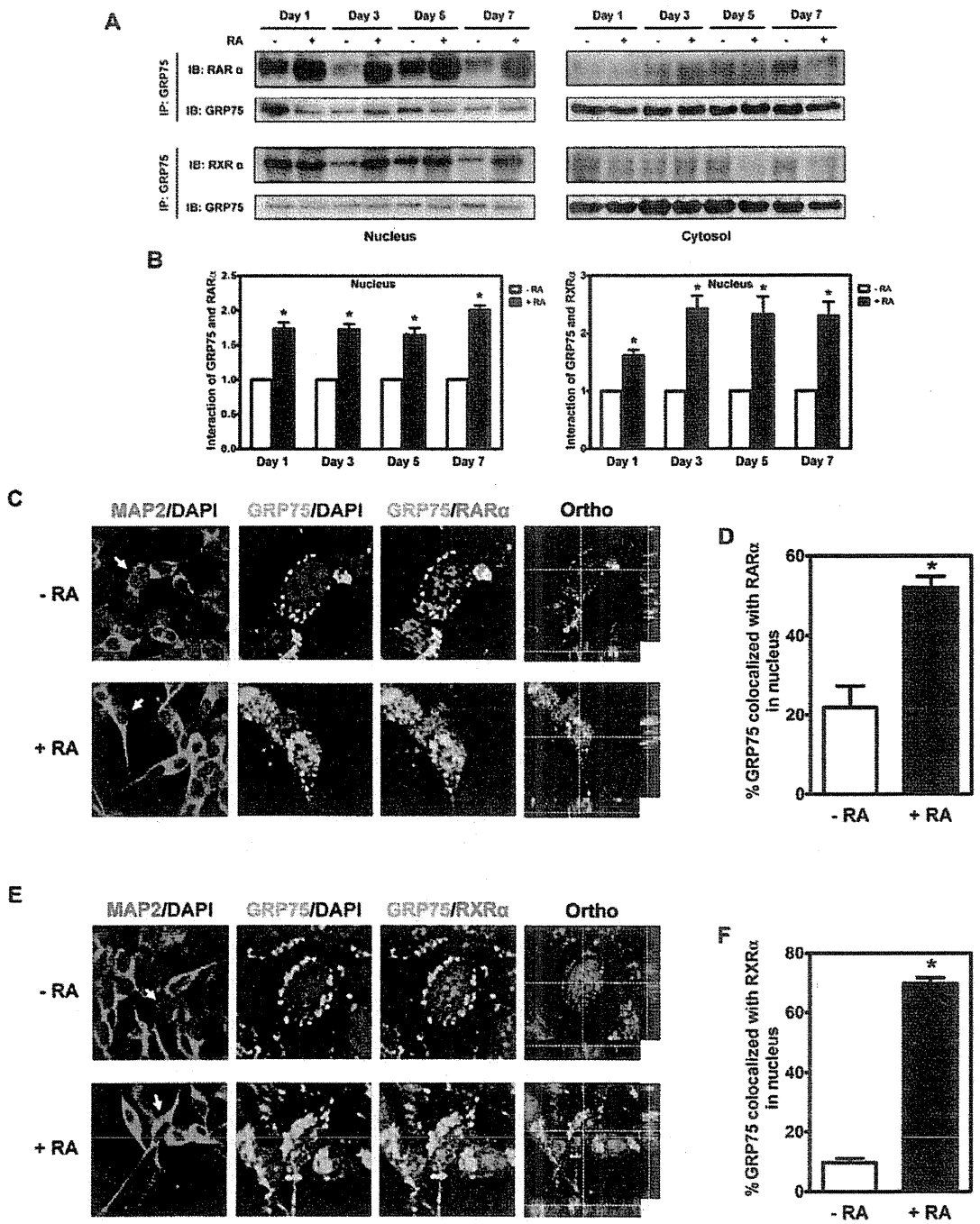

Figure 1. Nuclear GRP75 physically interacts with RARα/RXRα in differentiated NB cells. (A and B) Nuclear and cytoplasmic extracts were prepared from SH-SY5Y cells treated with RA (10 μM) or vehicle alone (0.1% DMSO) for various intervals. Clarified lysates of treated cells were subjected to immunoprecipitation using anti-GRP75 antibodies, followed by Western blot analysis with anti-RARα or RXRα. The levels of immunoprecipitated nuclear RARα and RXRα were normalized with those of nuclear GRP75 from the same immunopreciptate. The ratio of RARα or RXRα to GRP75 in DMSO-treated cells at a specific interval was referred to as 1 fold of relative interaction. Quantitative results are shown as the mean interactions of GRP75 with RARα or RXRα (±SEM) of three individual experiments and were analyzed by Student's t test. *$p<0.05$. (C-F) Immunofluorescence staining representing the colocalization between GRP75 and RARα/RXRα. SH-SY5Y cells were treated with RA (10 μM) or vehicle alone (0.1% DMSO) for 3 d and processed for immunofluorescence staining with anti-MAP2, anti-GRP75, and either anti-RARα or RXRα. Nuclei were visualized by DAPI counterstaining. Three-dimensional analysis of the co-localization of GRP75 and either RARα or RXRα by *z*-stack images was denoted by intersecting lines in the *x*, *y*, and *z* axes. Scale bar = 20 μm. Overlapped pixels (yellow) corresponding to GRP75 (green) and either RARα (C, red) or RXRα (E, red) were defined as the co-localization of GRP75 with either RARα or RXRα. The co-localization of GRP75 with either RARα (D) or RXRα (F) was determined as the mean (±SEM) percentages of nuclear GRP75-specific pixels overlapped with either RARα- or RXRα-specific pixels from at least three different viewing areas per experiment in three independent experiments and analyzed by Student's t test. *$p<0.05$.
doi:10.1371/journal.pone.0026236.g001

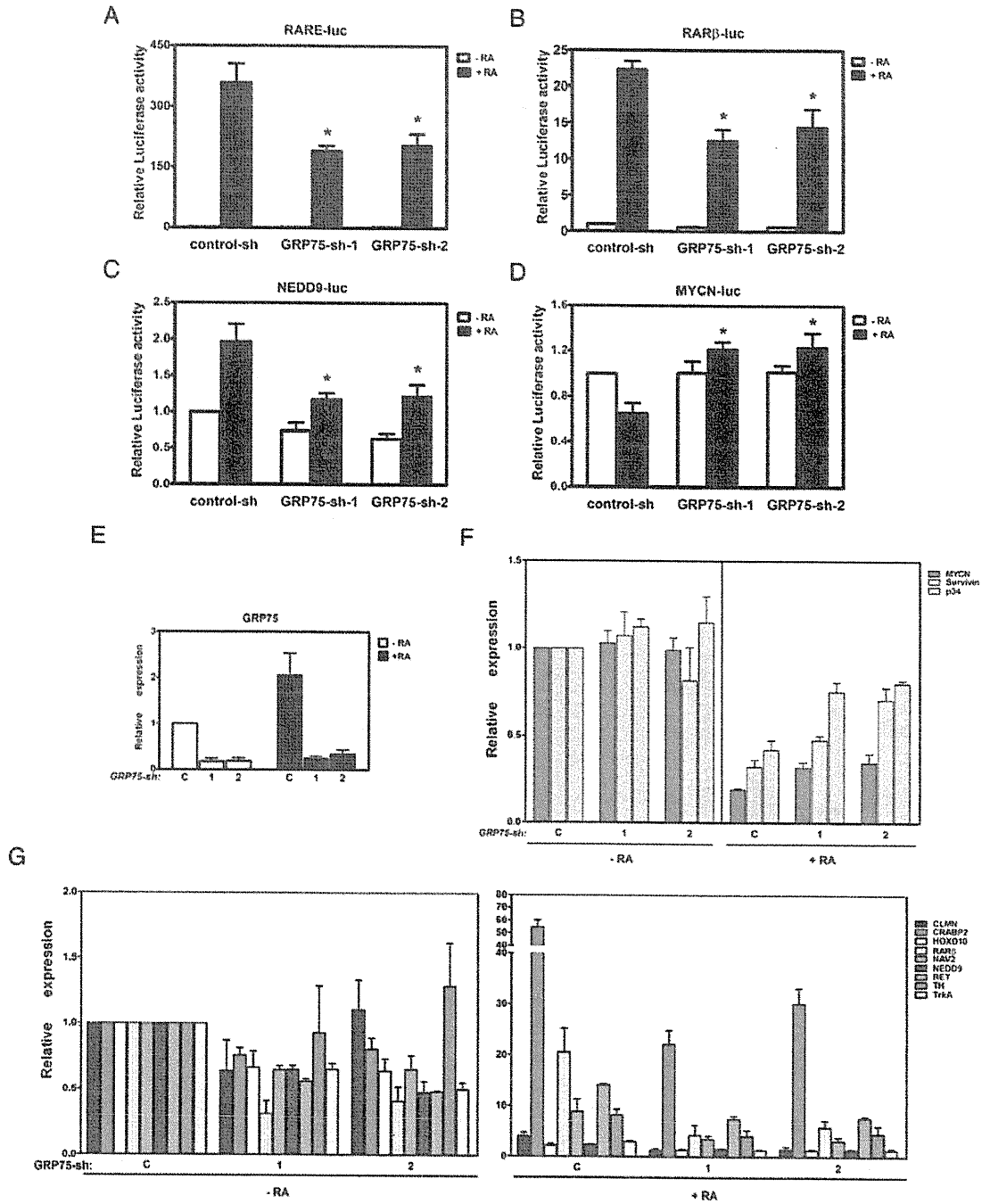

Figure 2. GRP75 is required for the transcriptional regulation of RA target genes in NB cells. (A–D) SH-SY5Y cells were infected with lentivirus encoding shRNA targeting GFP (Control-sh) or GRP75 (GRP75-sh-1 and -2) for 2 d, and infected cells were then transfected with RARE-Luc (A), *RARβ* promoter-Luc (B), NEDD9-Luc (C), or the MYCN-Luc (D) reporter gene construct for an additional 2 d. Following treatment with RA (10 μM) or vehicle alone (0.1% DMSO) for 24 h at 37°C, the luciferase signals in clarified lysates of treated cells were determined and normalized to protein concentration. Normalized luciferase signal of DMSO-treated Control-sh-infected cells were referred to as one fold of relative luciferase activity. (E) shRNA-infected SH-SY5Y cells treated with RA or DMSO as described above were harvested and processed for total RNA isolation by TRIzol reagent. The levels of GRP75 mRNA transcript as well as GAPDH (internal control) were determined by real-time RT-PCR. The normalized level of GRP75 transcript in Control-sh-infected DMSO-treated cells was referred to as 1 fold of relative GRP75 expression. Quantitative data were calculated as the mean (±SEM) relative GRP75 expression of triplicate measurements from three independent experiments and analyzed by Student's t test. (F-G) Total RNA transcripts of shRNA-infected SH-SY5Y cells treated with RA or DMSO were analyzed by real-time RT-PCR for the expression of RA target genes essential for cell proliferation (F) and neuronal differentiation (G). All quantitative data were calculated as the mean (±SEM) from three independent experiments and analyzed by Student's t test. *$p<0.05$.
doi:10.1371/journal.pone.0026236.g002

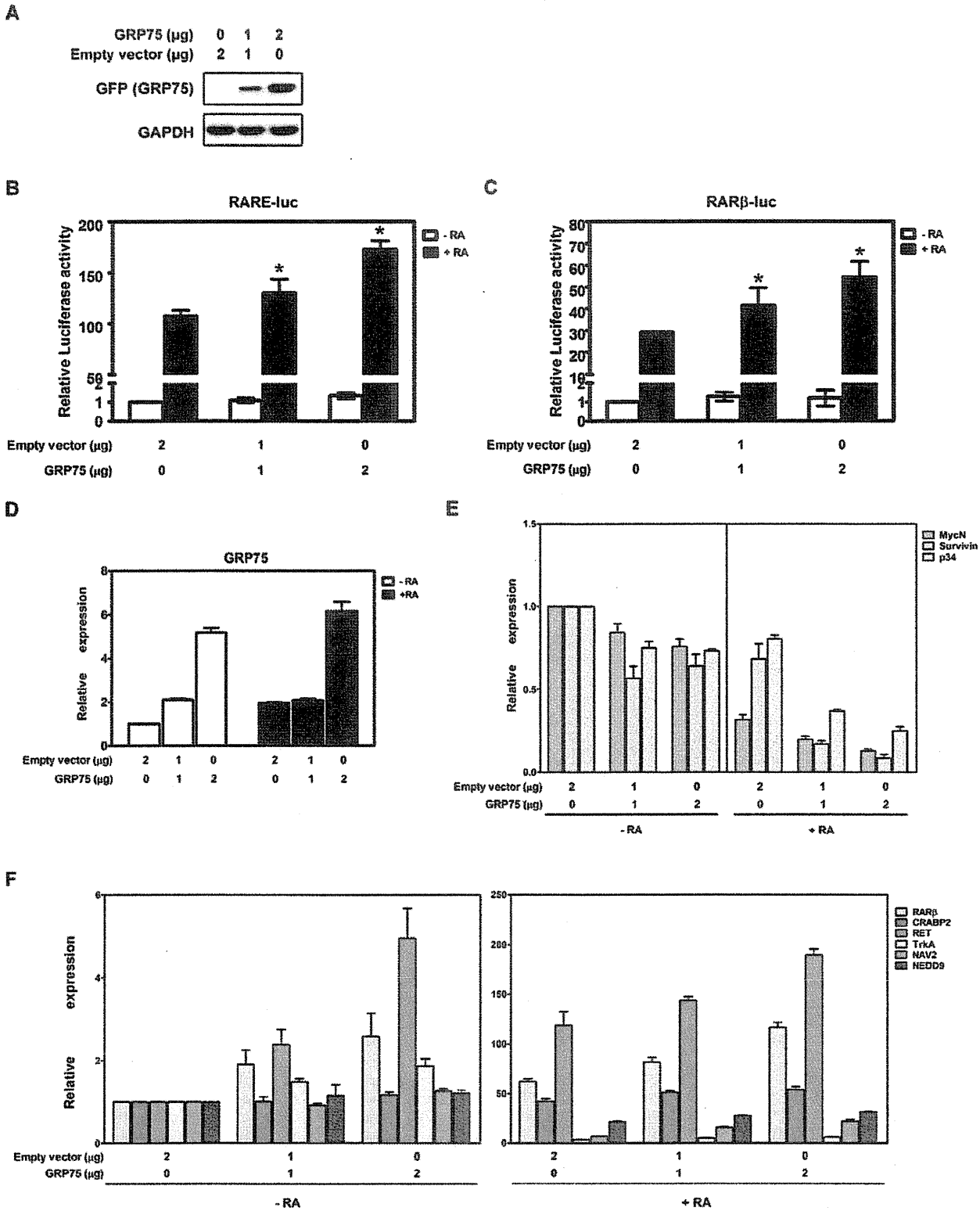

Figure 3. Overexpression of GRP75 augments RA-elicited activation of RARα/RXRα-mediated transcriptional regulation in SH-SY5Y cells. (A) SH-SY5Y cells were transiently transfected with an empty vector or a GRP75-expression vector for 24 h. Ectopic expression of GFP-GRP75 in RA-treated transfected cells was analyzed by Western blot analysis with anti-GFP antibody (upper panel, for GRP75). GAPDH (lower panel) was used as a protein loading control. (B and C) SH-SY5Y cells were transiently co-transfected with a RA-responsive reporter gene construct (2 μg of RARE-Luc or

RARβ-Luc) and a GRP75-expressing construct at various concentrations for 24 h, followed by treatment with 10 μM RA for 24 h. Luciferase signals derived from reporter gene constructs were determined by Steady-Glo luciferase assay reagents and normalized by protein concentration. The normalized luciferase signal in DMSO-treated cells transfected with an empty vector alone was referred to as 1 fold of relative luciferase activity. Quantitative results are presented as the mean (±SEM) of triplicate measurements from three independent experiments and were analyzed by Student's t test. *$p<0.05$. (D) The levels of GRP75 mRNA transcripts in SH-SY5Y cells transiently transfected with a GRP75-expressing vector were determined by quantitative real-time RT-PCR. The normalized level of GRP75 transcripts in DMSO-treated cells transfected with an empty vector alone was referred to as 1 fold of relative expression. Quantitative results are presented as the mean (±SEM) of triplicate measurements from three independent experiments. (E and F) SH-SY5Y cells were transfected with an empty vector or a GRP75-expressing vector for 48 h, followed by treatment with or without RA for 24 h. The transcript levels of various RA-responsive genes in transfected cells were determined by quantitative real-time RT-PCR. The normalized transcript level in DMSO-treated cells transfected with an empty vector alone was referred to as 1 fold of relative expression. Quantitative results are presented as the mean (±SEM) of triplicate measurements from three independent experiments and were analyzed by Student's t test.
doi:10.1371/journal.pone.0026236.g003

S9, and Figure S10). The present results clearly demonstrate for the first time that GRP75 can be actively involved in RARα/RXRα-mediated transcriptional regulation in RA-triggered neuronal differentiation of NB cells.

GRP75/RARα/RXRα complexes cooperatively bind to the retinoic acid response element (RARE) within the promoters of RA-responsive genes

To further demonstrate the functional role of the GRP75-bound RARα/RXRα receptor complex in RA-elicited transcriptional regulation, the RARα/RXRα-mediated binding to DR5 RARE within the promoter of *RARβ*, a direct target gene downstream of RA-elicited signaling [18], was examined using chromatin immunoprecipitation (ChIP) in SH-SY5Y cells infected with lentiviral particles expressing shRNAs targeting GFP (Control-sh) or GRP75 (GRP75-sh-1 and GRP75-sh-2) in the presence or absence of RA. The RNAi-mediated down-regulation of GRP75 significantly diminished the recruitment of RARα and RXRα receptors to RARE-containing promoter regions in RA-treated NB cells (Figure 4A), suggesting that GRP75 can be recruited to RARE consensus sequence within the promoter of *RARβ* and indispensable for the binding of RARα/RXRα receptor complexes to the promoters of RA target genes and that it critically modulates the RA-elicited expression of pro-differentiation genes. Since GRP75, RARα, and RXRα are all indispensable for cell viability, the depletion of GRP75 in SH-SY5Y cells in the absence of RA could compromise the basal viability of NB cells [9,25,26]. It is thus possible that the recruitment of RARα/RXRα to the RARE region could be enhanced to compensate the loss in GRP75-dependent maintenance of cell viability in response to GRP75 knockdown. These findings thus favor a model in which the binding of GRP75 is a prerequisite for the efficient association of RARα/RXRα complexes with RARE-containing promoter regions to modulate the expression of RA target genes in the regulation of neuronal differentiation.

Down-regulation of GRP75 promotes RARα/RXRα degradation through a proteasome-mediated pathway

Accumulated evidence also suggests that the ubiquitin proteasome system (UPS)-mediated degradation and the binding to molecular chaperones can modulate the activity of steroid receptors, including RAR/RXR retinoid receptor family [27,28,29,30]. We thus demonstrated that RNAi-mediated down-regulation of GRP75 in RA-treated SH-SY5Y cells resulted in a significant increase in the ubiquitination and UPS-mediated degradation of ligand-bound RARα/RXRα, compared to mock-infected cells (Figure 5). Consistent with its protective role, the overexpression of GRP75 resulted in a significant attenuation in the ubiquitination of both RARα and RXRα (Figure S5). Together, these findings suggest that GRP75-dependent increase in the stability of ligand-bound RARα/RXRα heterodimers could selectively potentiate ligand-bound RARα/RXRα-mediated transcriptional regulation, synergistically augmenting RA-elicited neuronal differentiation.

An enhanced interaction between GRP75 and RARα/RXRα heterodimers is associated with favorable outcomes in an in vivo xenograft NB mouse model

To validate the significance of the interaction between GRP75 and RARα/RXRα heterodimers in the modulation of RA-elicited neuronal differentiation *in vivo*, the correlation of these novel protein-protein interactions with tumor progression was examined in a xenograft NB mouse model [31]. We found that RA treatment significantly inhibits tumor growth beginning on the fourth treatment day until the completion of the treatment period in comparison to vehicle-treated control animals based on tumor size measurements. The assessment of harvested tumor xenografts at the conclusion of treatment revealed that both tumor size and tumor weight were significantly decreased in RA-treated mice (Tables S1), indicating that RA therapy can effectively inhibit the progression of NB. The correlation between the level of GRP75/RARα/RXRα tripartite complexes and tumor growth was further analyzed in the harvested NB xenografts. Our data showed that the association of GRP75 with either RARα or RXRα is significantly increased in RA-treated xenografts compared to controls (Figure 6, Table S1). Linear correlation analysis demonstrated that the formation of either GRP75/RARα or GRP75/RXRα complexes was markedly elevated in tumors with reduced volume or weight (RA-treated xenografts), in stark contrast to the control tumors with larger volume or weight (Figure S6). These results clearly demonstrate that the complex formation of tripartite GRP75/RARα/RXRα is inversely correlated with the progression of NB.

The interaction between GRP75 and RXRα/RARαis correlated with a higher grade of histological differentiation and a normal MYCN copy number in human NB tumors

To corroborate the relationship between the RA-induced formation of nucleus-localized GRP75/RARα/RXRα tripartite complexes with the differentiation of human NB, the interaction between GRP75 and RARα/RXRα heterodimers was examined in NB tumors with various grades of histological differentiation. Using co-immunoprecipitation with an anti-GRP75 antibody and lysates derived from 30 human NB tumors, including 13 ganglioneuroblastomas (GNBs), 9 differentiating NBs (DNBs), and 8 undifferentiated NBs (UNBs), the interaction between GRP75 and RARα/RXRα was found to be significantly stronger in tumors with higher grades of histological differentiation (GNB and DNB) than in those with an undifferentiated histology (UNB) (Figure 7A, B and Figure S8). Furthermore, the interaction

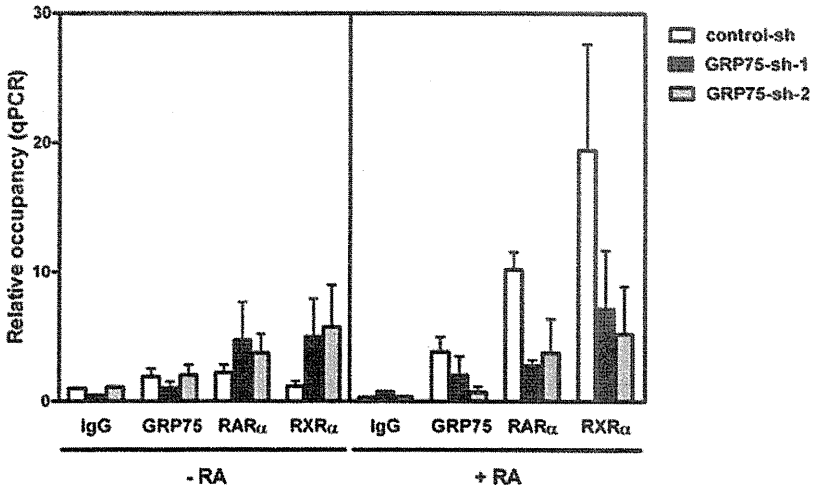

Figure 4. GRP75 is an obligatory constituent of RARα/RXRα-containing transcription machinery. (A) Down-regulation of GRP75 reduces the RA-elicited binding of RARα/RXRα heterodimers to the RARE motif. SH-SY5Y cells were infected by a lentivirus expressing control shRNA (Control-sh) or GRP75-targeting shRNAs (GRP75-sh-1 and -2) for 2 d. Infected cells were grown in the presence or absence of RA (10 μM) for 24 h. Soluble chromatins of treated cells were cross-linked by formaldehyde and sonicated to shear DNA. Protein-bound chromatin fragments were immunoprecipitated using a control mouse IgG antibody, mouse anti-GRP75, rabbit anti-RARα, or rabbit anti-RXRα antibody. The levels of DR5 RARE sequences within the RARβ promoter eluted from antibody-reactive immunoprecipitates were determined by quantitative real-time PCR. Sonicated total DNA fragments were used as the input DNA. The level of DR5 RARE normalized with input DNA in control IgG-reactive immunoprecipitates derived from DMSO-treated Control-sh-infected cells was referred to as one fold of relative occupancy. The results are shown as the mean (±SEM) from three independent experiments and were analyzed by Student's t test. $p<0.05$.
doi:10.1371/journal.pone.0026236.g004

between GRP75 and RARα/RXRα was higher in tumors with a normal MYCN copy number compared with those with MYCN amplification which carry a very unfavorable prognosis (Figure 7C, D). These pieces of evidence were consistent with our finding that GRP75 is required for RA-elicited down-regulation of MYCN expression (Figure 2D, F). The present data thus unequivocally support a model in which the level of tripartite GRP75/RARα/RXRα complexes in NB tumors is tightly associated with the histological grade of differentiation and, possibly, a favorable prognosis of NB tumors. Our data thus favors a model in which, upon RA-induced neuronal differentiation, GRP75 could be recruited to the ligand-bound RARα/RXRα heterodimers to cooperatively regulate the expression of RA downstream genes and avert UPS-mediated degradation of RA-bound RARα/RXRα (Figure S7A). Given that the molecular structure of human GRP75 has not been resolved, we then based on the structure of *Escherichia coli* HSP70 chaperone chain A (PubMed accession P0A6Y8, Protein Data Bank code 2KHO_A) that exhibits the highest amino acid sequence identity to human GRP75 to predict the three-dimensional model of GRP75. We then further simulated the possible docking of modeled GRP75 structure to known RARα or RXRα structure. This molecular simulation predicted that GRP75 could bind to the ligand-binding domain or the DNA-binding domain of RARα/RXRα heterodimers (Figure S7B, C). In conclusion, the present findings further strengthen the prognostic value of the expression level of GRP75 in NB [16], and delineate the mechanism underlying the GRP75-dependent regulation of RA-elicited RARα/RXRα-dependent neuronal differentiation.

Discussion

GRP75 has been shown to bind multiple partner proteins to govern diverse cellular functions [14,32]. The alteration in the cellular distribution of GRP75 could also correlate with the status of cellular immortality [33,34]. Consistent with this notion, our data clearly show that the association of GRP75 with RARα and RXRα is remarkably increased in the nucleus and coincides with the RA-elicited growth arrest, concomitant with a tight correlation between RA-induced nuclear translocation of GRP75 and RA-triggered neuronal differentiation. These data strongly favor a model in which nuclear GRP75 could stably form complexes with RARα/RXRα heterodimers and actively participate in RA-triggered neuronal differentiation of NB cells through the persistent modulation of RARα/RXRα activity (Figure S7).

The present data provide the first direct evidence that nucleus-localized GRP75 is essential for RARα/RXRα-mediated transcriptional regulation and that the GRP75/RARα/RXRα tripartite complexes physically bind to RARE to modulate the expression of RA target genes for neuronal differentiation (Figures 2, 3, 4). These results also support previous findings showing that RA-elicited down-regulation of MYCN expression is a prerequisite for the neuronal differentiation of NB cells, while constitutive overexpression of MYCN can counteract RA-induced neuronal differentiation [35,36]. GRP75 could thus play a central role in coordinating the transcriptional regulation of MYCN expression through the stimulation of RARα/RXRα activity, modulating a positive auto-regulatory loop for MYCN in NB cells [20]. GRP75 could also act as a transcriptional co-activator to potentiate RARα/RXRα-mediated transactivation of pro-differentiation genes, constituting a positive feedback loop that can potentiate RA-induced neuronal differentiation of NB cells. Consistent with the essential role of GRP75 in neuronal function [37], our results thus strengthen the notion that the functions of retinoid receptors, like other nuclear receptors, could be regulated by molecular chaperones, such as GRP75, in an evolutionarily conserved fashion [38,39,40].

The activity of nuclear receptors could be regulated by post-translational modifications, including phosphorylation and ubiquitination [41]. Previous studies have shown that phosphorylation of

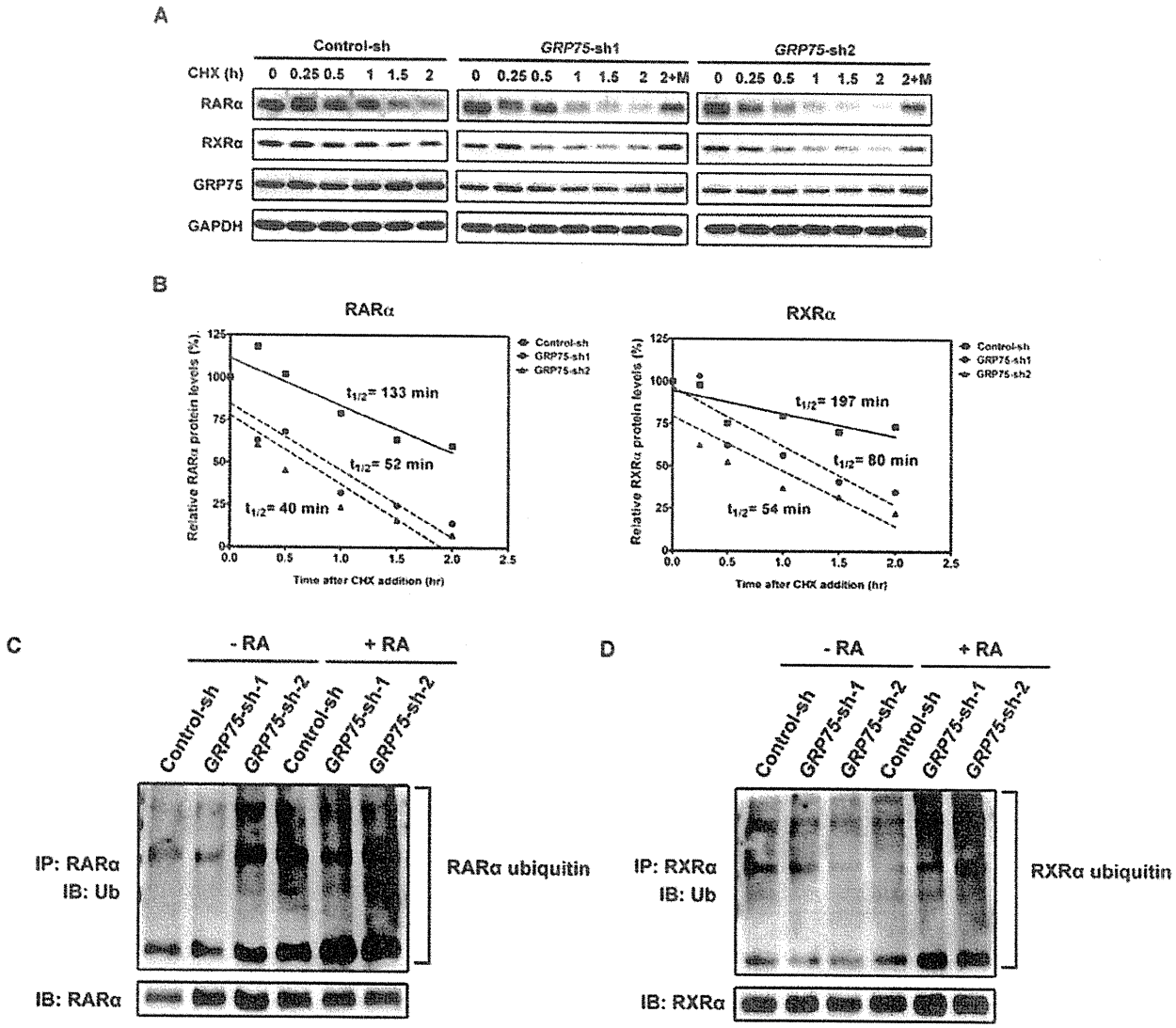

Figure 5. Deficiency in GRP75 promotes the degradation of RARα/RXRα heterodimers by the ubiquitin proteasome system. (A and B) SH-SY5Y cells were infected with a control shRNA (Control-sh) or GRP75-specific shRNAs (GRP75-sh-1 and -2) for 2 d. Cells were then treated with 50 μg/ml of cycloheximide (CHX) and 10 μM RA for various intervals. The protein levels of RARα, RXRα, GRP75, and GAPDH (protein load control) were analyzed by SDS-PAGE and immunoblotting (A). The relative levels of RARα (left panel) and RXRα (right panel) in infected cells prior to being treated with cycloheximide and RA were referred to as 100% (B). (C and D) SH-SY5Y cells infected with gene-targeting lentiviral shRNAs (Control-sh, GRP75-sh-1, and GRP75-sh-2) were treated with MG-132 (5 μM) in the presence or absence of RA (10 μM) for 16 h. Clarified lysates were subjected to immunoprecipitation with either anti-RARα or anti-RXRα. The ubiquitinated RARα (C) and RXRα (D) in immunoprecipitates were resolved by SDS-PAGE and visualized by immunoblotting with an anti-ubiquitin antibody. The same blots were reprobed with anti-RARα or anti-RXRα to reveal the input levels of both receptors (lower panel).
doi:10.1371/journal.pone.0026236.g005

RARs within their TFIIH binding sites is essential for RA-mediated embryonic development and underlies the pathogenesis of xeroderma pigmentosum [42]. RARs have also been shown to interact with SUG-1 to induce its ubiquitination and degradation by the proteasome upon RA stimulation [43]. A recent study revealed that Hsp27 can form a complex with androgen receptor (AR) and co-migrate into the nucleus to modulate the transcriptional activity of AR through an alteration in the UPS-mediated degradation of AR [28]. The activity of RA receptors was also shown to be modulated by interacting proteins, such as calreticulin [44]. Consistent with the functional roles of chaperones [45], the present results showing that GRP75 interacts with RARα and RXRα and is involved in the UPS-mediated degradation of these receptors further substantiate the idea that the magnitude and function of retinoid-elicited signaling could depend on the efficiency of the UPS-mediated processing of ligand-bound retinoid receptors (Figure 5 and Figure S5). A recent study showed that the molecular chaperone HSP90 binds to the E3 ubiquitin ligase CHIP and prevents CHIP-mediated degradation of leucine-rich repeat kinase 2 (LRRK2) [46]. The present findings that GRP75 could stabilize the RARα/RXRα complex by modulating the UPS pathway to potentiate the RA-elicited

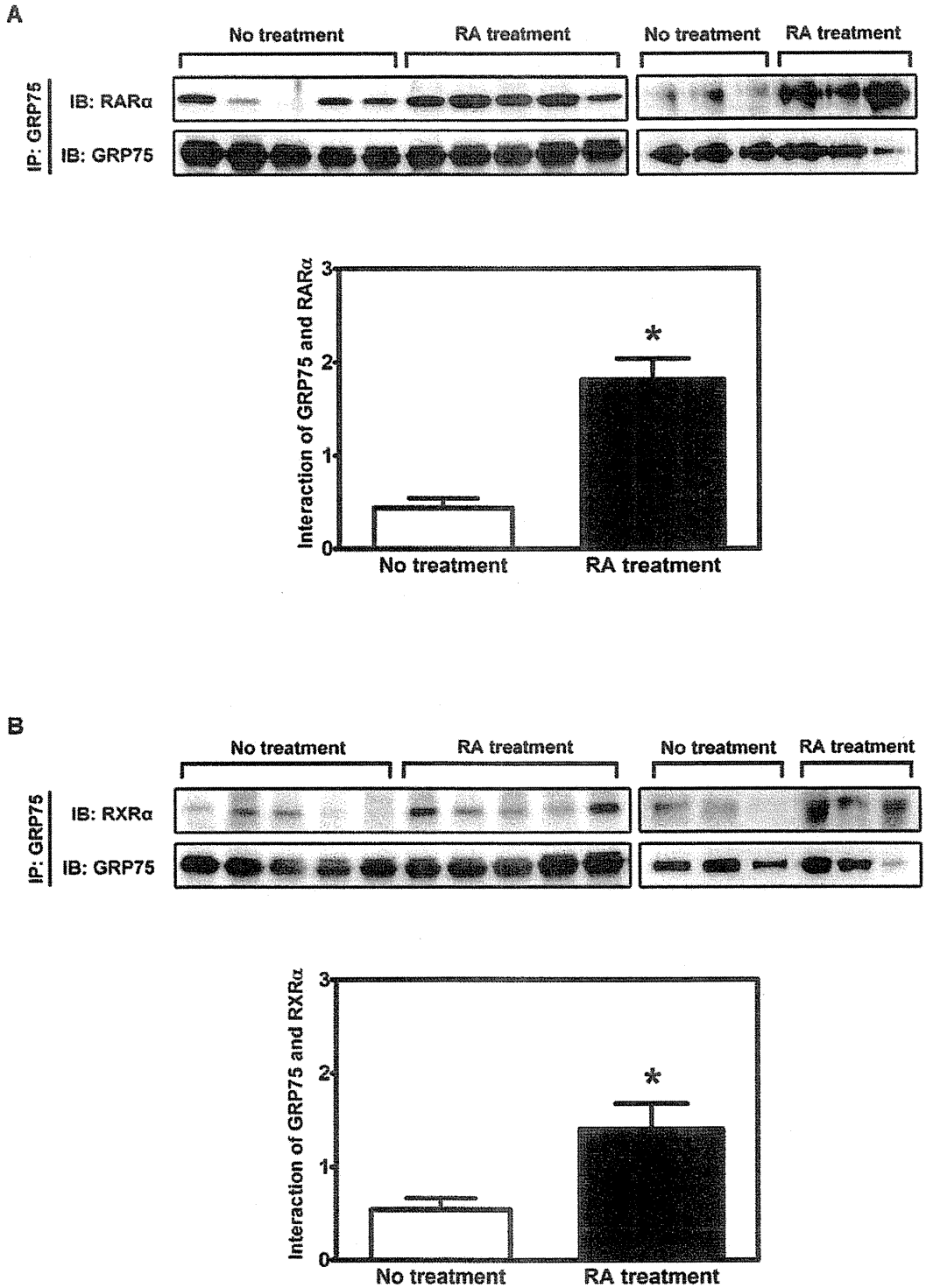

Figure 6. The interaction between GRP75 and RARα/RXRα is significantly increased in mouse NB xenografts treated with RA. Male nude mice were subcutaneously inoculated with 1×10^7 stNB-V1 NB cells with matrigel. Once the size of the xenograft tumor reached approximately 1 cm^3, tumor-bearing mice were intraperitoneally treated with RA (1 mg/kg b.w.) or vehicle (0.1% DMSO) daily for 14 d. Clarified lysates derived from xenograft tumors were subjected to immunoprecipitation with an anti-GRP75 antibody. Immunoprecipitated proteins were analyzed by SDS-PAGE and immunoblotting with anti-RARα (A) or RXRα (B). The same blots were reprobed with anti-GRP75 to reveal the input level of GRP75 (lower panel). The ratios of RARα to GRP75 (A) and RXRα to GRP75 (B) were referred to as the interaction between GRP75 and respective receptors. Quantitative results are shown as the mean (±SEM) of 8 xenografts from two independent experiments and were analyzed by Student's t test. *$p<0.05$.
doi:10.1371/journal.pone.0026236.g006

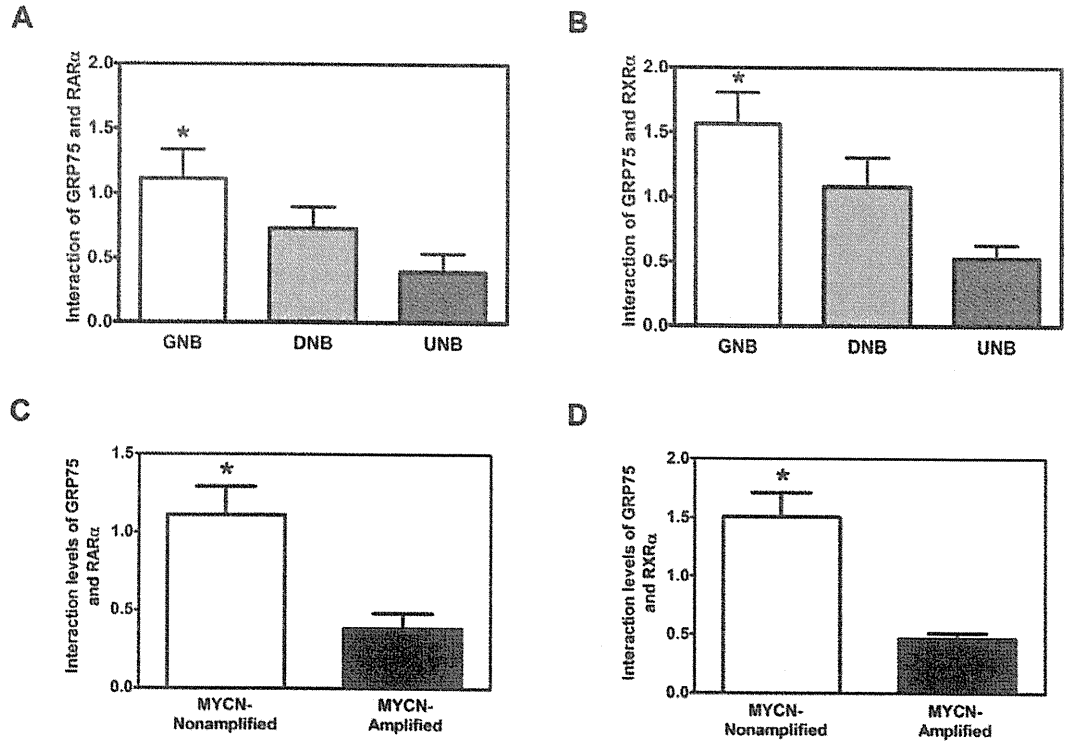

Figure 7. The interaction between GRP75 and RARα/RXRα in primary NB tumors is tightly associated with the differentiation histology but is inversely correlated with MYCN amplification. (A and B) Tumors collected from NB patients with different histology statuses, including ganglioneuroblastoma (GNB), differentiated neuroblastoma (DNB), and undifferentiated neuroblastoma (UNB), were processed for immunoprecipitation with anti-GRP75. The levels of GRP75-interacting RARα and RXRα in immunoprecipitates were analyzed by immunoblotting with anti-RARα (A) or anti-RXRα (B). The same blots were reprobed with anti-GRP75 to reveal the input level of GRP75. The ratios of RARα to GRP75 (A) and RXRα to GRP75 (B) were referred to as the interaction between GRP75 and the respective receptors. Quantitative results are shown as the mean (±SEM) interaction between GRP75 and RARα (A) or RXRα (B) and were analyzed by Student's t test. *$p<0.05$. The images of Western blots for the GRP75 immunoprecipitation used for this analysis wwer included in the Figure S8. Human NBs were classified by histology based on the criteria established by the International Neuroblastoma Pathology Classification [53]. GNB (n = 13); DNB (n = 9); UNB (n = 8). (C and D) The correlation between the levels of GRP75/RARα/RXRα complexes and MYCN status in primary NB tumors from the same cohort was determined. Quantitative data are shown as the mean (±SEM) interaction between GRP75 and RARα (C) or RXRα (D) in tumors without MYCN amplification (MYCN-nonamplified, n = 16) or those with MYCN amplification (MYCN-amplified, n = 5) and were analyzed by Student's t test. *$p<0.05$.
doi:10.1371/journal.pone.0026236.g007

neuronal differentiation of NB cells further support a critical role of the UPS pathway in the regulation of the activity of RA receptors [47].

The association between GRP75 and RARα/RXRα heterodimers is of clinical significance. In a xenograft mouse model of NB and a cohort of patient samples, the formation of tripartite GRP75/RARα/RXRα complexes was inversely correlated with tumor progression and consistently predicted a favorable outcome (Figure 6, Figure 7, Figure S6, and Table S1). Given that the N-terminal ATP-binding domain and the C-terminal substrate-binding domain of GRP75 are highly identical to those of human Hsp70 [48,49], GRP75 could act like Hsp70 and modulate the conformations of RARα and RXRα. Based on the molecular modeling for the interaction between GRP75 and either RARα or RXRα (Figure S7), GRP75 is likely to interact with either the ligand-binding domain or the DNA-binding domain of RARα/RXRα heterodimers to synergistically stabilize the RA-bound GRP75/RARα/RXRα complexes and sustain their transcriptional activation. Synthetic molecules designed to either induce the de novo formation of GRP75/RARα/RXRα complexes or stabilize the pre-existent ones could thus have profound therapeutic implication for NB.

In summary, the present study identifies a novel function of GRP75 in regulating RA-elicited neuronal differentiation through direct interaction with RARα/RXRα heterodimers in the nucleus. The elucidation of the molecular mechanism involved in the formation of tripartite GRP75/RARα/RXRα complexes provides the basis for the development of a novel therapeutic strategy for NB that could be combined with other existing differentiating regimens to improve the overall outcomes of NB patients [50,51]. Our data could serve as the foundation for the generation of molecules that could simultaneously prevent UPS-mediated degradation of RARα/RXRα and extend the pro-differentiation effect of GRP75/RARα/RXRα complexes.

Materials and Methods

Ethics Statement

The Institutional Review Board of National Taiwan University Hospital approved the complete follow-up protocols and this study. We obtained the written informed consent from all participants involved in this study. The animal study protocol used in this study was approved by the Institutional Animal Care and Use Committee of Academia Sinica (Approval Protocol ID

#TMiZOOLY2007092). Fetal bovine serum was obtained from Invitrogen (Carlsbad, CA).

Authentication of cell lines

The human NB cell lines SH-SY5Y (ATCC® CRL-2266™), SK-N-SH (ATCC® HTB-11™), SK-N-DZ (ATCC® CRL-2149™), SK-N-MC (ATCC® HTB-10™), and SK-N-BE(2) (ATCC® CRL-2271™) were obtained from American Type Culture Collection (Manassas, VA, USA) in November 2007. The human NB cell line IMR-32 (BCRC 60014) was obtained from Biosource Collection and Research Center (Hsinchu, Taiwan) in November 2007. These NB cell lines have been authenticated in our laboratory in a monthly basis. The SH-SY5Y and SK-N-SH cell lines were last authenticated by microscopic morphology check and PCR-based microplasma test in August 2011. The PCR-based microplasma testing was performed as previously described [50].

Immunofluorescence confocal microscopy

SH-SY5Y cells were grown on coverslips and treated with 10 μM RA in DMSO or 0.1% DMSO alone for the indicated time. Immunofluorescence staining was performed as described previously [16].

Reporter gene constructs and lentiviral shRNAs

The DR5-TK and RARβ-luciferase reporter constructs were kindly provided by Dr. Jonathan Kurie (The University of Texas M.D. Anderson Cancer Center) [52]. The Nedd9 promoter constructs were kindly provided by Dr. Margaret Clagett-Dame (University of Wisconsin-Madison) [19]. The shRNA lentiviral vectors targeting human GRP75 (GRP75-sh-1 and GRP75-sh-2) and a GFP-targeting control lentiviral vector (Control-sh) were purchased from the National RNAi Core Facility, Academia Sinica, Taiwan.

Co-immunoprecipitation and Western blotting

The nuclear extracts and cytosolic pools of treated cells were isolated using the Nuclei EZ Prep Kit (Sigma) as described in the manufacturer's instructions. For co-immunoprecipitation, 20 μg of goat anti-GRP75 antibody was incubated with 200 μl of immobilized protein A agarose in PBS for 2 h at 4°C. Immunoprecipitated proteins were eluted by the addition of 4X sample loading buffer and boiling at 100°C for 10 min, followed by SDS-PAGE and Western blotting.

Luciferase reporter assay

shRNA-transduced cells were transfected with a promoter-specific luciferase reporter gene construct (either RARE-luc, RARβ-luc, NEDD9-luc, or MYCN-luc) using Lipofectamine 2000 at 37°C overnight. Promoter-driven luminescence in the clarified lysates of transfected cells was determined using the Steady-Glo luciferase assay reagent (Promega) and normalized to the protein content of the lysates.

RNA isolation, reverse transcription, and quantitative real-time PCR

Total RNA was isolated from transduced SH-SY5Y cells using the TRIzol Reagent (Invitrogen). Purified RNAs (2 μg) were reverse-transcribed to the first-strand cDNA using the SuperScript III First-strand cDNA Synthesis Kit (Invitrogen). Equivalent amounts of cDNA were used in quantitative real-time PCR using the SYBR Green I Master reagent on the LightCycler 480 Real-Time PCR System (Roche) with gene-specific primer pairs.

Chromatin immunoprecipitation (ChIP)

Treated cells were fixed with 1% formaldehyde for 10 min at 37°C, and the reaction was terminated by the addition of 1.25 M glycine (1:9, v/v). Fixed cells were lysed and sonicated in buffer A (1% SDS, 10 mM EDTA, 50 mM Tris, pH 8.0) to shear DNA. Clarified lysates were subject to immunoprecipitation using antibodies (10 μg) against either GRP75, RARα, RXRα, or mouse IgG (as control) at 4°C overnight with agitation, followed by incubation with protein A-conjugated agarose at 4°C for 1 h.

Protein stability

Protein synthesis in infected cells was inhibited with 50 μg/ml cycloheximide for 3 h, followed by the addition of 10 μM RA or vehicle alone (0.1% DMSO) and incubation at 37°C for various intervals.

Ubiquitination assay for RARα and RXRα

SH-SY5Y cells were infected with GRP75-sh-1, GRP75-sh-2, or control-sh at 37°C for 2 d, followed by the removal of infection mixture and incubation with fresh medium containing 10 μM RA or 0.1% DMSO for 16 h in the presence or absence of 5 μM MG132.

Patients and sample preparation

A cohort of 30 histologically confirmed NB patients with complete follow-up protocols approved by the Institutional Review Board of National Taiwan University Hospital, Taipei, Taiwan, were enrolled in this study. The Institutional Review Board of National Taiwan University Hospital also approved this study, and we obtained informed written consent from all participants involved in this study. Tumor samples were obtained during surgery and immediately frozen in liquid nitrogen. The categorization of tumor biopsies was based on the International Neuroblastoma Pathology Classification scheme [53].

Additional information regarding details of individual experimental procedures can be found in the Supplemental Methods S1 submitted along with the main manuscript.

Supporting Information

Figure S1 GRP75 is translocated into the nucleus of differentiated neuroblastoma cells. (A) Immunofluorescence microscopy analysis of GRP75 in the nuclei of NB cells. SH-SY5Y cells were treated with or without RA (10 μM) for 3 d and processed for immunofluorescence staining with an anti-GRP75 antibody (green). Nuclei were counterstained with DAPI (blue). Insets, two-fold magnification of highlighted cells (arrow). Scale bar = 20 μm. (B) Three-dimensional analysis of individual cells by *z*-stack confocal images at specific sites marked by intersecting lines in the *x*, *y*, and *z* axes. (C) Quantitative analysis of the intensity of cells double labeled for GRP75 and DAPI (nuclear DNA). Data are expressed as the average percentage (±SEM) of nuclear GRP75 co-localized with RARa from three independent experiments. *$p<0.05$. (D) The nuclear extracts of SH-SY5Y cells treated with or without RA for various intervals were resolved by SDS-PAGE and analyzed by immunoblotting with the indicated antibodies. Histone H1 and Lamin A/C were markers for nuclear extracts, while GAPDH was included as a protein loading control for cytosolic pools. The prolonged exposure for GAPDH blot (Nucleus) revealed no contamination of cytosolic proteins in the isolated nuclear extracts. Similarly, overexposure of histone H1- and lamin A/C-labeled blots (Cytosol) showed that isolated cytosolic pools were free from contamination of nuclear proteins. (TIF)

Figure S2 The interaction between GRP75 and RARα/RXRα is increased in RA-treated SH-SY5Y cells. (A) SH-SY5Y cells were grown on coverslips and treated with 10 μM RA for various intervals. Cells treated with vehicle alone (0.1% DMSO) were included as controls. Treated cells were fixed with 4% paraformaldehyde and subjected to immunofluorescence staining using goat anti-GRP75 (green), mouse anti-MAP2 (red), and rabbit anti-RARα (red). Nuclei were counterstained with DAPI. The inset shows the magnification of the highlighted region (arrow). Scale bar = 20 μm. (B) The levels of nuclear GRP75 were quantified using MetaMorph Offline 7.5.1.0 Image Analysis System (Molecular Devices). Quantitative results are shown as the mean (±SEM) from three independent experiments. (C) The levels of GRP75 co-localized with RARα in the nucleus were quantified using the MetaMorph Offline 7.5.1.0 Image Analysis System (Molecular Devices). Quantitative data are shown as means (±SEM) of at least three different viewing areas from three independent experiments. All quantitative data were analyzed by Student's t test. *$p<0.05$ versus DMSO-treated control (− RA). (D) SH-SY5Y cells were treated with 10 μM RA for various intervals. Cells treated with vehicle alone (0.1% DMSO) were included as controls (− RA). Treated cells were fixed with 4% paraformaldehyde and subjected to immunofluorescence staining using goat anti-GRP75 (green), mouse anti-MAP2 (red), and rabbit anti-RXRα (red). Nuclei were visualized by DAPI staining. The inset shows the magnified view of the highlighted region (arrow). Scale bar = 20 μm. (E and F) The levels of nuclear GRP75 (E) and RXRα-co-localized GRP75 in the nucleus (F) were determined using the MetaMorph Offline 7.5.1.0 Image Analysis System (Molecular Devices). Quantitative results are shown as means (±SEM) from three independent experiments and were analyzed by Student's t test. *$p<0.05$ versus DMSO-treated control (− RA). The number of cells used in the quantitative analysis was at least 150.
(TIF)

Figure S3 RA enhances the formation of GRP75/RARα/RXRα tripartite complexes in various NB cell lines. MYCN-nonamplified NB cell lines, including SK-N-SH (A), SK-N-MC (B), and stNB-V1 (C), and MYCN-amplified NB cell lines, including SK-N-BE (D), SK-N-DZ (E), and IMR-32 (F), were treated with 10 μM RA or vehicle alone (0.1% DMSO) for 1 d. Nuclear lysates were immunoprecipitated with a mouse anti-GRP75 antibody. Protein A-bound antigen-antibody complexes were analyzed by immunoblotting with anti-RARα (upper panel), anti-RXRα (middle panel), or anti-GRP75 (lower panel, loading control). The levels of RARα and RXRα were normalized to GRP75 from the same immunoprecipitate, and those in cells without RA treatment were referred to as one fold of relative interaction between GRP75 and respective RA receptors (RARα and RXRα).
(TIF)

Figure S4 Lentiviral shRNA-mediated down-regulation of GRP75 in SH-SY5Y cells. SH-SY5Y cells were infected with lentiviral shRNA targeting GFP (Control-sh) or GRP75 (GRP75-sh-1 and -2) for 2 d, followed by treatment with 10 μM RA or vehicle alone (0.1% DMSO) for 1 d. Clarified lysates containing equivalent amounts of proteins were analyzed by Western blotting with anti-GRP75 (upper panel) or GAPDH (lower panel, protein load control).
(TIF)

Figure S5 Overexpression of GRP75 in SH-SY5Y cells decreases the ubiquitination of RARα and RXRα in response to RA signaling. SH-SY5Y cells were transiently transfected with an GRP75-expressing vector or an empty vector for 48 h, followed by treatment with 10 μM of MG132 in the presence or absence of 10 μM RA for an additional 16 h. Clarified lysates were subjected to immunoprecipitation with a rabbit anti-RARα (A) or anti-RXRα (B) antibody. Proteins pulled down by immunoprecipitation were resolved by SDS-PAGE and analyzed by immunoblotting with an anti-ubiquitin antibody. The same blots were stripped and re-probed with anti-RARα (A, lower panel) or anti-RXRα (B, lower panel) to visualize the individual receptors as loading controls.
(TIF)

Figure S6 The interaction between GRP75 and RARα/RXRα heterodimers was inversely correlated to tumor volume and tumor weight in a xenograft NB mouse model. The interaction between GRP75 and RARα/RXRα in xenograft NB tumors harvested from mice treated with RA (solid bar) or saline (open bar) was determined as described in Fig. 6 of the main text. The ratio of RARα to GRP75 (A) or RXRα to GRP75 (B) in individual xenografts was normalized to tumor volume (left panel) or tumor weight (right panel). Quantitative results are shown as the means (±SEM) from xenografts in controls (no treatment, $n = 8$) or treated animals (RA treatment, $n = 8$) and were analyzed by Student's t test. *$p<0.05$.
(TIF)

Figure S7 A model delineating the GRP75-mediated regulation of RA-elicited neuronal differentiation through direct interaction with RARα/RXRα and the structure modeling predicting interaction interfaces between GRP75 and RARα/RXRα. (A) The model illustrates that GRP75 could act as a cofactor of RARα/RXRα to mediate RA-triggered neuronal differentiation. Upon RA stimulation, GRP75 could be recruited to the ligand-bound RARα/RXRα heterodimers and cooperatively regulate the expression of RA downstream genes, resulting in enhanced neuronal differentiation. Simultaneously, RA-bound GRP75/RARα/RXRα tripartite complexes could avert UPS-mediated degradation, extending the RA-elicited transactivation of RARα/RXRα to induce neuronal differentiation. (B and C) Structure modeling predicts that GRP75 could bind to the ligand-binding domain (B) or the DNA-binding domain (C) of RARα/RXRα heterodimers. White, GRP75; Green, RARα; Blue, RXRα; Yellow and pink, double strand DNA.
(TIF)

Figure S8 The binding of GRP75 to RARα or RXRα is elevated in NB patients with favorable outcome. The levels of GRP75/RARα/RXRα complexes in 30 primary tumors with various histologies was analyzed by immunoprecipitation with a mouse anti-GRP75 antibody, followed by immunoblotting with indicated antibodies. Corresponding quantitative analysis of these blots was shown in the Figure 7 of main text. GNB, ganglioneuroblastoma ($n = 13$, G1~G13); DNB, differentiated neuroblastoma ($n = 9$, D1~D9); UNB, undifferentiated neuroblastoma ($n = 8$, U1~U8).
(TIF)

Figure S9 Down-regulation of GRP75 abrogates RA-elicited transcriptional activation of RA receptors in SK-N-SH cells. (A–D) SK-N-SH cells were infected with lentivirus encoding shRNA targeting GFP (Control-sh) or GRP75 (GRP75-sh-1 and -2) for 2 d. The knockdown efficiency was verified by immunoblotting (A) or real-time RT-PCR (inset in F). For promoter assay, the infected cells were additionally transfected with RARE-Luc (B), *RARβ* promoter-Luc (C), NEDD9-Luc (D), or

the MYCN-Luc (E) reporter gene construct for an additional 2 d. Following treatment with RA (10 μM) or vehicle alone (0.1% DMSO) for 24 h at 37°C, the luciferase signals in clarified lysates of treated cells were determined and normalized with protein concentration. Normalized luciferase signal of DMSO-treated Control-sh-infected cells were referred to as one fold of relative luciferase activity. (F-G) Infected SK-N-SH cells treated with RA or DMSO as described above were harvested and processed for total RNA isolation by TRIzol reagent. Total RNA transcripts of shRNA-infected SK-N-SH cells treated with RA or DMSO were analyzed by real-time RT-PCR for the expression of RA target genes essential for cell proliferation (F) and neuronal differentiation (G). The normalized level of GRP75 transcript in Control-sh-infected DMSO-treated cells was referred to as 1 fold of relative expression. All quantitative data were calculated as the mean (±SEM) from three independent experiments and analyzed by Student's t test. *$p<0.05$.
(TIF)

Figure S10 Overexpression of GRP75 strengthens RA-elicited activation of RA receptors in SK-N-SH cells. (A) SK-N-SH cells were transiently transfected with an empty vector or a GRP75-expression vector for 24 h. Ectopic expression of GFP-GRP75 in RA-treated transfected cells was analyzed by Western blot analysis with anti-GFP antibody (upper panel, for GRP75). GAPDH (lower panel) was used as a protein loading control. (B and C) SK-N-SH cells were transiently co-transfected with a RA-responsive reporter gene construct (2 mg of RARE-Luc or RARβ-Luc) and a GRP75-expressing construct at various concentrations for 24 h, followed by treatment with 10 μM RA for 24 h. Luciferase signals derived from reporter gene constructs were determined by Steady-Glo luciferase assay reagents and normalized by protein concentration. The normalized luciferase signal in DMSO-treated cells transfected with an empty vector alone was referred to as 1 fold of relative luciferase activity. Quantitative results are presented as the mean (±SEM) of triplicate measurements from three independent experiments and were analyzed by Student's t test. *$p<0.05$. (D) The levels of GRP75 mRNA transcripts in SK-N-SH cells transiently transfected with a GRP75-expressing vector were determined by quantitative real-time RT-PCR. The normalized level of GRP75 transcripts in DMSO-treated cells transfected with an empty vector alone was referred to as 1 fold of relative expression. Quantitative results are presented as the mean (±SEM) of triplicate measurements from three independent experiments. (E and F) SK-N-SH cells were transfected with an empty vector or a GRP75-expressing vector for 48 h, followed by treatment with or without RA for 24 h. The transcript levels of various RA-responsive genes in transfected cells were determined by quantitative real-time RT-PCR. The normalized transcript level in DMSO-treated cells transfected with an empty vector alone was referred to as 1 fold of relative expression. Quantitative results are presented as the mean (±SEM) of triplicate measurements from three independent experiments and were analyzed by Student's t test.
(TIF)

Figure S11 The specificity of the mouse anti-GRP75 antibody for co-immunoprecipitation is validated in cultured cells, tumor xenograft, and human primary NB tumors. The cellular lysates (nuclear and cytosolic fractions, A), homogenates derived from xenografted tumors of mice (B), and clarified extracts derived from human primary NB tumors with different histological grades of differentiation (C) were immunoprecipitated with a mouse anti-GRP75 or a mouse control IgG. The GRP75-bound proteins were analyzed by Western blotting with a goat anti-GRP75, rabbit anti-RARα or rabbit anti-RXRα antibody, respectively. In (C), G, ganglioneuroblastoma; D, differentiated neuroblastoma; U, undifferentiated neuroblastoma.
(TIF)

Figure S12 RA induces nuclear translocation of GRP75 in SK-N-BE and SK-N-SH cells. SK-N-DZ (A) and SK-N-SH (B) cells were treated with 10 μM RA for 24 h, the nuclear lysates were subject to Western blot analysis. The levels of nuclear GRP75 were normalized with those of histone H1. The normalized level of GRP75 in cells without RA treatment was referred to as one fold of relative nuclear translocation. All quantitative data were calculated as the mean (±SEM) from three independent experiments.
(TIF)

Figure S13 RA treatments induce the nuclear translocation of GRP75 in a dose-dependent manner. SH-SY5Y cells were treated with various concentrations of RA (0.1, 1, and 10 μM) for 24 h, and the nuclear extracts derived from treated cells were analyzed by immunoblotting with an anti-GRP75 or anti-histone H1 (protein loading control of nuclear fraction) antibody. The levels of nuclear GRP75 were normalized with those of histone H1. The normalized level of GRP75 in cells treated with vehicle alone (0.1% DMSO) was referred to as one fold of nuclear GRP75. All quantitative data were calculated as the mean (±SEM) from three independent experiments.
(TIF)

Table S1 The levels of GRP75-bound RARα and RXRα in xenografts in comparison to tumor volume and tumor weight in mice treated with RA or vehicle.
(DOC)

Methods S1 Additional information regarding details of individual experimental procedures.
(DOC)

Acknowledgments

We are extremely thankful to Drs. Chi-Huey Wong and Y.-S. Edmond Cheng (Genomic Research Center, Academia Sinica) for their generous support. The authors are indebted to Mr. Ching-Yao Su (Academia Sinica) for assistance with the preparation of shRNA lentiviruses. We would like to thank Dr. Jonathan Kurie (The University of Texas M.D. Anderson Cancer Center) for providing the DR5-luc and RARβ-luc reporter gene constructs and Dr. Margaret Clagett-Dame (University of Wisconsin-Madison) for providing the Nedd9 promoter constructs. We also thank the Core Facility of the Institute of Cellular and Organismic Biology, Academia Sinica, for technical support. The shRNA lentiviral vectors were obtained from the National RNAi Core Facility located at the Institute of Molecular Biology/Genomic Research Center, Academia Sinica.

Author Contributions

Conceived and designed the experiments: Y-YS C-YP W-MH Y-FL. Performed the experiments: Y-YS W-MH Y-MJ H-FJ. Analyzed the data: Y-YS W-MH Y-FL. Contributed reagents/materials/analysis tools: HL AN Y-GT D-TL F-JH. Wrote the paper: Y-YS W-MH Y-FL.

References

1. Maris JM (2010) Recent advances in neuroblastoma. N Engl J Med 362: 2202–2211.
2. Wagner LM, Danks MK (2009) New therapeutic targets for the treatment of high-risk neuroblastoma. J Cell Biochem 107: 46–57.
3. Sidell N, Altman A, Haussler MR, Seeger RC (1983) Effects of retinoic acid (RA) on the growth and phenotypic expression of several human neuroblastoma cell lines. Exp Cell Res 148: 21–30.
4. Brodeur GM (2003) Neuroblastoma: biological insights into a clinical enigma. Nat Rev Cancer 3: 203–216.
5. Matthay KK, Reynolds CP, Seeger RC, Shimada H, Adkins ES, et al. (2009) Long-term results for children with high-risk neuroblastoma treated on a randomized trial of myeloablative therapy followed by 13-cis-retinoic acid: a children's oncology group study. J Clin Oncol 27: 1007–1013.
6. Park JR, Villablanca JG, London WB, Gerbing RB, Haas-Kogan D, et al. (2009) Outcome of high-risk stage 3 neuroblastoma with myeloablative therapy and 13-cis-retinoic acid: a report from the Children's Oncology Group. Pediatr Blood Cancer 52: 44–50.
7. Matthay KK, Villablanca JG, Seeger RC, Stram DO, Harris RE, et al. (1999) Treatment of high-risk neuroblastoma with intensive chemotherapy, radiotherapy, autologous bone marrow transplantation, and 13-cis-retinoic acid. Children's Cancer Group. N Engl J Med 341: 1165–1173.
8. Reynolds CP, Schindler PF, Jones DM, Gentile JL, Proffitt RT, et al. (1994) Comparison of 13-cis-retinoic acid to trans-retinoic acid using human neuroblastoma cell lines. Prog Clin Biol Res 385: 237–244.
9. Maden M (2007) Retinoic acid in the development, regeneration and maintenance of the nervous system. Nat Rev Neurosci 8: 755–765.
10. Lefebvre P, Martin PJ, Flajollet S, Dedieu S, Billaut X, et al. (2005) Transcriptional activities of retinoic acid receptors. Vitam Horm 70: 199–264.
11. Bastien J, Rochette-Egly C (2004) Nuclear retinoid receptors and the transcription of retinoid-target genes. Gene 328: 1–16.
12. McGrane MM (2007) Vitamin A regulation of gene expression: molecular mechanism of a prototype gene. J Nutr Biochem 18: 497–508.
13. Niederreither K, Dolle P (2008) Retinoic acid in development: towards an integrated view. Nat Rev Genet 9: 541–553.
14. Deocaris CC, Widodo N, Ishii T, Kaul SC, Wadhwa R (2007) Functional significance of minor structural and expression changes in stress chaperone mortalin. Ann N Y Acad Sci 1119: 165–175.
15. Wadhwa R, Taira K, Kaul SC (2002) An Hsp70 family chaperone, mortalin/mthsp70/PBP74/Grp75: what, when, and where? Cell Stress Chaperones 7: 309–316.
16. Hsu WM, Lee H, Juan HF, Shih YY, Wang BJ, et al. (2008) Identification of GRP75 as an independent favorable prognostic marker of neuroblastoma by a proteomics analysis. Clin Cancer Res 14: 6237–6245.
17. Mark M, Ghyselinck NB, Chambon P (2006) Function of retinoid nuclear receptors: lessons from genetic and pharmacological dissections of the retinoic acid signaling pathway during mouse embryogenesis. Annu Rev Pharmacol Toxicol 46: 451–480.
18. de The H, Vivanco-Ruiz MM, Tiollais P, Stunnenberg H, Dejean A (1990) Identification of a retinoic acid responsive element in the retinoic acid receptor beta gene. Nature 343: 177–180.
19. Knutson DC, Clagett-Dame M (2008) atRA Regulation of NEDD9, a gene involved in neurite outgrowth and cell adhesion. Arch Biochem Biophys 477: 163–174.
20. Suenaga Y, Kaneko Y, Matsumoto D, Hossain MS, Ozaki T, et al. (2009) Positive auto-regulation of MYCN in human neuroblastoma. Biochem Biophys Res Commun 390: 21–26.
21. Balmer JE, Blomhoff R (2002) Gene expression regulation by retinoic acid. J Lipid Res 43: 1773–1808.
22. Merrill RA, Ahrens JM, Kaiser ME, Federhart KS, Poon VY, et al. (2004) All-trans retinoic acid-responsive genes identified in the human SH-SY5Y neuroblastoma cell line and their regulated expression in the nervous system of early embryos. Biol Chem 385: 605–614.
23. Jeong H, Kim MS, Kim SW, Kim KS, Seol W (2006) Regulation of tyrosine hydroxylase gene expression by retinoic acid receptor. J Neurochem 98: 386–394.
24. Merrill RA, Plum LA, Kaiser ME, Clagett-Dame M (2002) A mammalian homolog of unc-53 is regulated by all-trans retinoic acid in neuroblastoma cells and embryos. Proc Natl Acad Sci U S A 99: 3422–3427.
25. Craig EA, Kramer J, Shilling J, Werner-Washburne M, Holmes S, et al. (1989) SSC1, an essential member of the yeast HSP70 multigene family, encodes a mitochondrial protein. Mol Cell Biol 9: 3000–3008.
26. Kawai A, Nishikawa S, Hirata A, Endo T (2001) Loss of the mitochondrial Hsp70 functions causes aggregation of mitochondria in yeast cells. J Cell Sci 114: 3565–3574.
27. Smith DF, Toft DO (2008) Minireview: the intersection of steroid receptors with molecular chaperones: observations and questions. Mol Endocrinol 22: 2229–2240.
28. Zoubeidi A, Zardan A, Beraldi E, Fazli L, Sowery R, et al. (2007) Cooperative interactions between androgen receptor (AR) and heat-shock protein 27 facilitate AR transcriptional activity. Cancer Res 67: 10455–10465.
29. Zhao HL, Ueki N, Marcelain K, Hayman MJ (2009) The Ski protein can inhibit ligand induced RARalpha and HDAC3 degradation in the retinoic acid signaling pathway. Biochem Biophys Res Commun 383: 119–124.
30. Boudjelal M, Wang Z, Voorhees JJ, Fisher GJ (2000) Ubiquitin/proteasome pathway regulates levels of retinoic acid receptor gamma and retinoid X receptor alpha in human keratinocytes. Cancer Res 60: 2247–2252.
31. Almgren MA, Henriksson KC, Fujimoto J, Chang CL (2004) Nucleoside diphosphate kinase A/nm23-H1 promotes metastasis of NB69-derived human neuroblastoma. Mol Cancer Res 2: 387–394.
32. Kaul SC, Taira K, Pereira-Smith OM, Wadhwa R (2002) Mortalin: present and prospective. Exp Gerontol 37: 1157–1164.
33. Wadhwa R, Pereira-Smith OM, Reddel RR, Sugimoto Y, Mitsui Y, et al. (1995) Correlation between complementation group for immortality and the cellular distribution of mortalin. Exp Cell Res 216: 101–106.
34. Wadhwa R, Sugihara T, Yoshida A, Nomura H, Reddel RR, et al. (2000) Selective toxicity of MKT-077 to cancer cells is mediated by its binding to the hsp70 family protein mot-2 and reactivation of p53 function. Cancer Res 60: 6818–6821.
35. Peverali FA, Orioli D, Tonon L, Ciana P, Bunone G, et al. (1996) Retinoic acid-induced growth arrest and differentiation of neuroblastoma cells are counteracted by N-myc and enhanced by max overexpressions. Oncogene 12: 457–462.
36. Thiele CJ, Reynolds CP, Israel MA (1985) Decreased expression of N-myc precedes retinoic acid-induced morphological differentiation of human neuroblastoma. Nature 313: 404–406.
37. Gabriele N, Pontoriero GF, Thomas N, Shethwala SK, Pristupa ZB, et al. (2010) Knockdown of mortalin within the medial prefrontal cortex impairs normal sensorimotor gating. Synapse 64: 808–813.
38. Dedhar S, Rennie PS, Shago M, Hagesteijn CY, Yang H, et al. (1994) Inhibition of nuclear hormone receptor activity by calreticulin. Nature 367: 480–483.
39. Burns K, Duggan B, Atkinson EA, Famulski KS, Nemer M, et al. (1994) Modulation of gene expression by calreticulin binding to the glucocorticoid receptor. Nature 367: 476–480.
40. Michalak M, Burns K, Andrin C, Mesaeli N, Jass GH, et al. (1996) Endoplasmic reticulum form of calreticulin modulates glucocorticoid-sensitive gene expression. J Biol Chem 271: 29436–29445.
41. Rochette-Egly C (2003) Nuclear receptors: integration of multiple signalling pathways through phosphorylation. Cell Signal 15: 355–366.
42. Keriel A, Stary A, Sarasin A, Rochette-Egly C, Egly JM (2002) XPD mutations prevent TFIIH-dependent transactivation by nuclear receptors and phosphorylation of RARalpha. Cell 109: 125–135.
43. Gianni M, Bauer A, Garattini E, Chambon P, Rochette-Egly C (2002) Phosphorylation by p38MAPK and recruitment of SUG-1 are required for RA-induced RAR gamma degradation and transactivation. EMBO J 21: 3760–3769.
44. Desai D, Michalak M, Singh NK, Niles RM (1996) Inhibition of retinoic acid receptor function and retinoic acid-regulated gene expression in mouse melanoma cells by calreticulin. A potential pathway for cyclic AMP regulation of retinoid action. J Biol Chem 271: 15153–15159.
45. Heinlein CA, Chang C (2001) Role of chaperones in nuclear translocation and transactivation of steroid receptors. Endocrine 14: 143–149.
46. Ding X, Goldberg MS (2009) Regulation of LRRK2 stability by the E3 ubiquitin ligase CHIP. PLoS One 4: e5949.
47. Perissi V, Rosenfeld MG (2005) Controlling nuclear receptors: the circular logic of cofactor cycles. Nat Rev Mol Cell Biol 6: 542–554.
48. Daugaard M, Rohde M, Jaattela M (2007) The heat shock protein 70 family: Highly homologous proteins with overlapping and distinct functions. FEBS Lett 581: 3702–3710.
49. Mayer MP (2010) Gymnastics of Molecular Chaperones. Mol Cell 39: 321–331.
50. Chang HH, Lee H, Hu MK, Tsao PN, Juan HF, et al. (2010) Notch1 expression predicts an unfavorable prognosis and serves as a therapeutic target of patients with neuroblastoma. Clin Cancer Res 16: 4411–4420.
51. Liao YF, Wang BJ, Hsu WM, Lee H, Liao CY, et al. (2007) Unnatural amino acid-substituted (hydroxyethyl)urea peptidomimetics inhibit gamma-secretase and promote the neuronal differentiation of neuroblastoma cells. Mol Pharmacol 71: 588–601.
52. Srinivas H, Xia D, Moore NL, Uray IP, Kim H, et al. (2006) Akt phosphorylates and suppresses the transactivation of retinoic acid receptor alpha. Biochem J 395: 653–662.
53. Shimada H (2003) The International Neuroblastoma Pathology Classification. Pathologica 95: 240–241.

VOLUME 29 · NUMBER 33 · NOVEMBER 20 2011

JOURNAL OF CLINICAL ONCOLOGY

ORIGINAL REPORT

Prognostic Value of the Stage 4S Metastatic Pattern and Tumor Biology in Patients With Metastatic Neuroblastoma Diagnosed Between Birth and 18 Months of Age

Denah R. Taggart, Wendy B. London, Mary Lou Schmidt, Steven G. DuBois, Tom F. Monclair, Akira Nakagawara, Bruno De Bernardi, Peter F. Ambros, Andrew D.J. Pearson, Susan L. Cohn, and Katherine K. Matthay

Denah R. Taggart, Steven G. DuBois, and Katherine K. Matthay, University of California San Francisco School of Medicine and Benioff Children's Hospital, San Francisco, CA; Wendy B. London, Dana-Farber Cancer Institute/Children's Hospital, Boston, MA; Mary Lou Schmidt, University of Illinois; Susan L. Cohn, University of Chicago, Chicago, IL; Tom F. Monclair, Rikshospitalet University Hospital, Oslo, Norway; Akira Nakagawara, Chiba Cancer Center, Chiba, Japan; Bruno De Bernardi, Istituto Giannina Gaslini, Genova, Italy; Peter F. Ambros, Children's Cancer Research Institute, St Anna Kinderkrebsforschung, Vienna, Austria; and Andrew D.J. Pearson, Institute of Cancer Research, Sutton, United Kingdom.

Submitted March 15, 2011; accepted July 25, 2011; published online ahead of print at www.jco.org on October 3, 2011.

Supported in part by National Institutes of Health Grant No. T32 CA128583-01, William Guy Forbeck Research Foundation, Dougherty Foundation, Conner Research Fund, Campini Foundation, and Mildred V. Strouss Professorship.

Presented in part at the 45th Annual Meeting of the American Society of Clinical Oncology, May 29-June 2, 2009, Orlando, FL.

Authors' disclosures of potential conflicts of interest and author contributions are found at the end of this article.

Corresponding author: Katherine K. Matthay, MD, Department of Pediatrics, UCSF School of Medicine, 505 Parnassus Ave, Box 0106, San Francisco, CA 94143-0106; e-mail: matthayk@peds.ucsf.edu.

0732-183X/11/2933-4358/$20.00

DOI: 10.1200/JCO.2011.35.9570

ABSTRACT

Purpose
Patients with neuroblastoma younger than 12 months of age with a 4S pattern of disease (metastases limited to liver, skin, bone marrow) have better outcomes than infants with stage 4 disease. The new International Neuroblastoma Risk Group (INRG) staging system extends age to 18 months for the 4S pattern. Our aim was to determine which prognostic features could be used for optimal risk classification among patients younger than 18 months with metastatic disease.

Methods
Event-free survival (EFS) and overall survival were analyzed by log-rank tests, Cox models, and survival tree regression for 656 infants with stage 4S neuroblastoma younger than 12 months of age and 1,019 patients with stage 4 disease younger than 18 months of age in the INRG database.

Results
Unfavorable biologic features were more frequent in infants with stage 4 disease than in infants with 4S tumors and higher overall in those age 12 to 18 months (although not different for stage 4 *v* 4S pattern). EFS was significantly better for infants younger than 12 months with 4S pattern than with stage 4 disease ($P < .01$) but similar for toddlers age 12 to 18 months with stage 4 versus 4S pattern. Among 717 patients with stage 4S pattern, patients age 12 to 18 months had worse EFS than those age younger than 12 months ($P < .01$). *MYCN*, 11q, mitosis-karyorrhexis index (MKI), ploidy, and lactate dehydrogenase were independently statistically significant predictors of EFS and more highly predictive than age or metastatic pattern. *MYCN*, 11q, MKI, histology, and 1p were combined in a survival tree for improved risk stratification.

Conclusion
Tumor biology is more critical than age or metastatic pattern for prognosis of patients age younger than 18 months with metastatic neuroblastoma and should be considered for risk stratification.

J Clin Oncol 29:4358-4364. © 2011 by American Society of Clinical Oncology

INTRODUCTION

Stage 4S neuroblastoma is a unique category of metastatic disease in infants. Originally described in 1971,[1] the definition (clarified by International Neuroblastoma Staging System [INSS]) categorizes infants younger than 12 months of age with metastases limited to the liver, skin, and bone marrow (< 10% replacement with tumor cells) as having stage 4S disease, hereafter referred to as 4S pattern. The primary tumor must be localized (INSS 1 or 2), without infiltration across the midline or contralateral lymph node involvement.[2]

Patients with 4S disease (7% to 10% of neuroblastoma)[3] have a more favorable outcome than other patients with metastatic neuroblastoma, often demonstrating spontaneous maturation and regression. Estimated survival rates of 70% to 90% have been reported, and these tumors are usually associated with favorable biologic features.[4-7] Unfortunately, a subgroup of patients with stage 4S disease and unfavorable prognostic features—including *MYCN* amplification, chromosomal aberrations (loss of heterozygosity [LOH] 1p, aberration 11q, gain 17q), diploidy, and age younger than 2 months at diagnosis—has significantly worse outcomes.[3,4,8-14]

The upper age limit defining 4S disease has been debated as a result of recent reports demonstrating more favorable outcomes for patients with metastatic

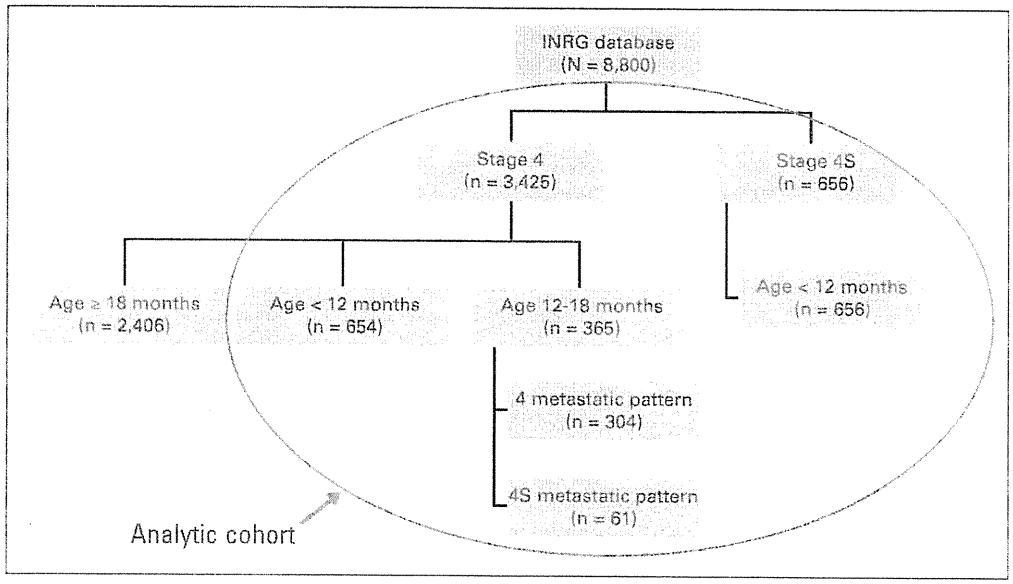

Fig 1. Analytic cohort. INRG, International Neuroblastoma Risk Group.

neuroblastoma diagnosed between 12 and 18 months of age.[15,16] Recently, the International Neuroblastoma Risk Group (INRG) developed consensus guidelines for a modified staging system based on clinical and radiologic criteria. The INRG increased the upper limit of age from 12 to 18 months for 4S disease (now designated Ms), defined as metastases limited to skin, liver, and bone marrow (< 10%) without cortical bone involvement and either L1 or L2 stage tumors, including large unresectable primary tumors that cross the midline.[17] These patients were then stratified by biologic features for risk classification. The current study uses the INRG database of 1,675 patients with metastatic neuroblastoma age 0 to 18 months to determine whether biologic and clinical features better than the younger-than-12-months age cutoff and 4S metastatic pattern can be identified to categorize patients with good outcomes.

METHODS

Patients

The INRG database contains information on 8,800 unique patients who provided consent for and were enrolled onto cooperative clinical trials between January 1, 1990, and December 31, 2002, by cooperative groups from multiple countries.[17] Requirements for eligibility into the INRG database include confirmed pathologic diagnosis of neuroblastoma excluding ganglioneuroma,[18] age 21 years or younger at diagnosis, and available data for disease and survival outcomes.

From this database, we identified 3,425 patients with INSS stage 4 and 656 patients with INSS stage 4S disease (Fig 1). Among patients with stage 4 disease, 654 were age younger than 12 months (infants) and 365 were age 12 to 18 months (toddlers) at diagnosis. With regard to patients with stage 4S disease, all 656 were younger than 12 months of age (by definition). These 1,675 patients formed our analytic cohort. We divided the patients with stage 4 disease age 12 to 18 months into two groups—those with (n = 61) and without (n = 304) 4S pattern of metastasis—independent of size of primary tumor or extent of bone marrow involvement.

Statistical Considerations

Factors evaluated in tests of association and survival analyses were as follows: *MYCN* gene amplification,[19,20] 11q aberration, 1p aberration, ploidy, grade, mitosis-karyorrhexis index (MKI), lactic dehydrogenase (LDH), primary site (adrenal *v* not adrenal), and initial treatment (surgery and observation *v* more intensive therapies). Both 11q and 1p chromosomal abnormalities were detected using fluorescence in situ hybridization or polymerase chain reaction. Using flow cytometry, ploidy was reported as less than or equal to one or more than one; all patients with more than one were classified as hyperdiploid. Histology is often used to categorize tumors as favorable or unfavorable. Because the INPC and Shimada classification systems incorporate age into their categorization, there is a duplication of the prognostic contribution when both age and histology are used as risk factors.[18,21] Therefore, we used tumor grade (differentiated *v* poorly or undifferentiated) and MKI (low or intermediate *v* high) to evaluate tumor histology. For LDH, median value was used to dichotomize the cohort; LDH less than 580 U/L was classified as low, and 580 U/L or greater was classified as high.

Fisher's exact tests were performed for prognostic factors versus metastatic pattern. For event-free survival (EFS), time to event was calculated as time from enrollment to first occurrence of relapse, progressive disease, secondary malignancy, or death as a result of any cause or to time of last patient contact, if no event occurred. For overall survival (OS), time to event was time from enrollment until death or time of last contact, if alive. Survival was estimated using the Kaplan-Meier method,[22] and subgroups were compared by log-rank test. EFS and OS are expressed as the 5-year estimate plus or minus SE.[23]

A Cox model on EFS was used to explore the possibility of a better age cutoff to define stage 4S disease.[24] The subset of 717 patients with stage 4S metastatic pattern (ie, including some stage 4 patients > 1 year of age) was repeatedly divided into two age groups. *P* values and hazard ratios for older versus younger patients were calculated, whereby the optimal age cutoff was statistically significant and maximized the difference in EFS between older and younger patients (ie, largest hazard ratio). The selected age cutoff was used in other Cox models to test binary age in combination with one biologic factor at time, and another model was used to identify all factors independently predictive of EFS.

Survival tree regression was used to determine if biologic factors could improve risk groupings for patients younger than 18 months of age with metastases, either in addition to or in combination with age and metastatic pattern.[21,25,26] Proportional hazards assumption was confirmed by visual inspection of survival curves and plots of log(time) versus log[−log(S[time])].

RESULTS

EFS and OS by Age and Pattern of Metastases

In the overall cohort of patients age 0 to 18 months with metastases, 5-year EFS and OS (± SE) were 70% ± 2% and 75% ± 1%,

respectively (Table 1). Five-year EFS was significantly higher for patients with 4S pattern of metastases (77% ± 2%) compared with patients with stage 4 pattern of metastases (64% ± 2%; $P < .001$; Table 1; Fig 2A). Five-year EFS was also significantly higher for stage 4S pattern age younger than 12 months (79% ± 2%) than for stage 4 pattern age younger than 12 months (70% ± 2%; $P < .001$; Fig 2B). In contrast, EFS for toddlers age 12 to 18 months with stage 4S pattern (55% ± 8%) was not significantly different from EFS for toddlers with stage 4 pattern (50% ± 4%; $P = .39$; Fig 2C). EFS was also improved for younger patients age younger than 12 months compared with that for patients age 12 to 18 months, overall (Fig 2D), and within each metastatic pattern (Figs 2E, 2F). OS paralleled EFS in all cases.

Table 1. EFS and OS in Patients With Metastatic Neuroblastoma < 18 Months of Age (n = 1,675)

Characteristic	Patients No.	Patients %	5-Year EFS ± SE (%)	5-Year EFS P	5-Year OS ± SE (%)	5-Year OS P
All patients	1,675		70 ± 2		75 ± 1	
Pattern of metastatic disease				< .001		< .001
Stage 4S	717	43	77 ± 2		84 ± 2	
Stage 4	958	57	64 ± 2		69 ± 2	
Age, months				< .001		< .001
< 12	1,310	78	75 ± 2		82 ± 1	
12-18	365	22	51 ± 3		53 ± 3	
MYCN amplification				< .001		< .001
No	1,070	79	83 ± 2		90 ± 1	
Yes	282	21	28 ± 4		32 ± 4	
Unknown	323					
Ploidy				< .001		< .001
> 1 (hyperdiploid)	548	73	81 ± 3		87 ± 2	
≤ 1 (diploid, hypodiploid)	206	27	59 ± 6		63 ± 6	
Unknown	921					
Histology				< .001		< .001
Favorable	592	79	86 ± 2		92 ± 2	
Unfavorable	156	21	38 ± 6		39 ± 6	
Unknown	927					
MKI				< .001		< .001
Low, intermediate	513	84	84 ± 2		90 ± 2	
High	100	16	38 ± 7		38 ± 7	
Unknown	1,062					
11q				.0376		.55
Normal	145	80	77 ± 6		84 ± 5	
Aberration	36	20	54 ± 16		83 ± 13	
Unknown	1,494					
1p				< .001		< .001
Normal	284	73	83 ± 3		91 ± 3	
Aberration	105	27	43 ± 7		49 ± 7	
Unknown	1,286					
LDH, U/L				< .001		< .001
< 587	427	43	83 ± 2		91 ± 2	
≥ 587	555	57	60 ± 3		64 ± 3	
Unknown	693					
Initial treatment				< .001		< .001
Surgery and observation	254	21	86 ± 3		95 ± 2	
Chemotherapy and transplantation	967	79	64 ± 2		71 ± 2	
Unknown	454					
Primary tumor location				.0011		< .001
Nonadrenal primary	586	36	75 ± 2		81 ± 2	
Adrenal primary	1,022	64	67 ± 2		72 ± 2	
Unknown	67					
Grade of neuroblastoma differentiation				.79		.53
Differentiating	54	8	76 ± 6		83 ± 5	
Undifferentiated	590	92	75 ± 3		81 ± 3	
Unknown	1,031					

Abbreviations: EFS, event-free survival; LDH, lactic dehydrogenase; MKI, mitosis-karyorrhexis index; OS, overall survival.

Distribution of Clinical and Biologic Characteristics

To understand these differences in outcome, we assessed associations of age and pattern of metastases with poor prognostic features (Table 2). For patients with stage 4S pattern, the proportion of patients with unfavorable features was significantly higher among toddlers (age 12 to 18 months) than infants (age < 12 months) for *MYCN* amplification, 1p aberration, unfavorable histology, high MKI, and high LDH. However, the proportion with adrenal primary was higher for patients age younger than 12 months than for those age 12 to 18 months. In comparing infants versus toddlers within the subgroup with stage 4 pattern, a significantly higher proportion of patients age 12 to 18 months had unfavorable features: *MYCN* amplification, diploidy, unfavorable histology, and high MKI. In contrast to stage 4S pattern, in stage 4 pattern, more toddlers than infants had an adrenal primary.

In infants, unfavorable biologic prognostic features were also significantly more frequent in stage 4 than stage 4S pattern, including *MYCN* amplification, diploidy, 1p aberration, unfavorable histology, high MKI, and high LDH. Adrenal primary was observed in more infants with stage 4S pattern compared with stage 4 pattern. In contrast, the proportion of unfavorable prognostic features was not significantly different between toddlers with stage 4 and toddlers with 4S pattern, except for adrenal primary, which was more common in stage 4 pattern.

The following subgroups had a significantly higher proportion of patients who received initial treatment with chemotherapy or other intensive therapy: among infants, more stage 4 than 4S pattern; toddlers, more stage 4S than stage 4 pattern; within stage 4S pattern, more toddlers than infants.

EFS and OS by Prognostic Factors

In the cohort of patients age 0 to 18 months with metastatic disease, univariate analyses revealed that both EFS and OS were statistically significantly worse for toddlers and patients with stage 4 pattern, *MYCN* amplification, diploidy, unfavorable histology, high MKI, 1p LOH or aberration, high LDH, and adrenal primary (Table 1; Appendix Tables A1-A4, online only). EFS was worse for patients with 11q LOH or aberration ($P = .0376$), but OS was not ($P = .55$). Patients whose initial treatment plan included chemotherapy or more intensive therapy had lower EFS ($P < .001$) and OS ($P < .001$; Table 1). Grade of differentiation did not seem to affect prognosis in this cohort and was excluded from the other analyses.

Distribution of Outcome by Age

We next evaluated the prognostic impact of age within the cohort of patients with metastatic disease age 0 to 18 months. Five-year EFS for patients younger than age 19 days with metastatic disease was less than 71% for all subgroups; the subgroup with the lowest EFS was made up of those 7 to 18 days of age with stage 4 pattern (58% at 5 years; Appendix Fig A1, online only). The most favorable outcomes were in patients diagnosed at 19 to 38 days of age. Thereafter, EFS gradually decreased with increasing

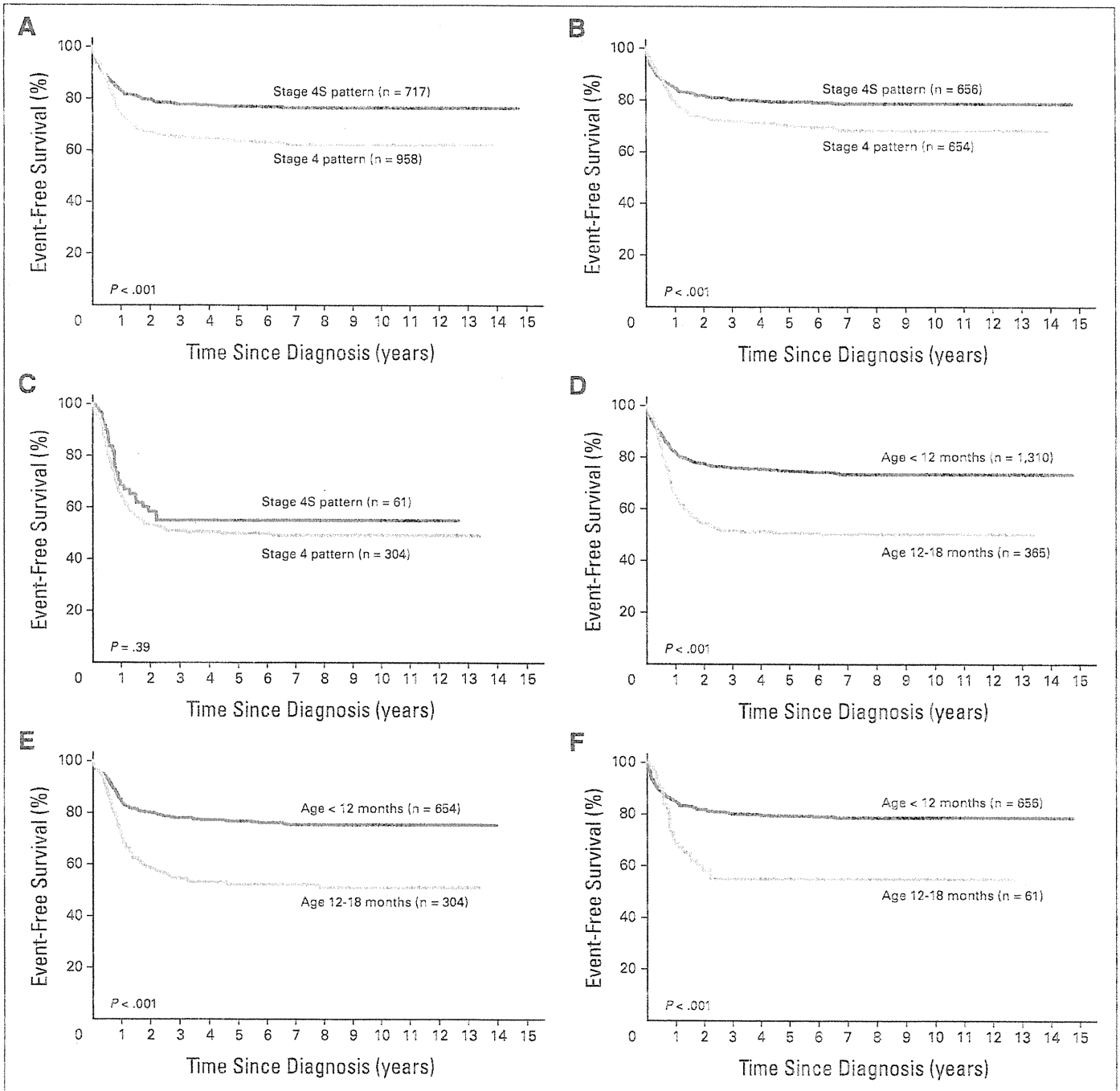

Fig 2. Event-free survival (EFS) comparisons by age and stage. EFS by stage for (A) all patients age 0 to 18 months with metastatic disease (n = 1,675), (B) infants age younger than 12 months (n = 1,310), and (C) toddlers age 12 to 18 months (n = 365). EFS by age for (D) all patients (n = 1,675), (E) patients with stage 4 pattern (n = 958), and (F) patients with stage 4S pattern (n = 717).

age in both 4 and 4S pattern, although EFS was lower for stage 4 pattern in almost every age group (Appendix Fig A1).

Within the cohort of patients with 4S pattern, we sought to determine whether the 365-day age cutoff maximized the outcome difference between younger and older patients. For patients with 4S pattern, those younger than 19 days of age had a 1.5 times greater risk of an event than patients 20 to 547 days of age, and those 365 days of age or older had a 2.31 times greater risk of an event than those who were younger than 365 days of age (Appendix Table A5, online only). No optimal age cutoff was identified, because the maximum hazard ratio was for the oldest group; risk for an event gradually increased with increasing age. Any choice of age cutoff greater than 226 days would be reasonable, so we made no change to the existing 365-day cutoff.

Multivariable Analysis

In univariate analyses, all factors were statistically significantly predictive of EFS except for grade of differentiation (Table 1). Significance of each factor was maintained when each was tested in combination with age in a multivariable Cox model (ie, testing to see if age and given factor were independently predictive of EFS; Table 3). In a

Table 2. Association of Risk Factors by Pattern of Metastases Within Age Subgroups and by Age Within Pattern of Metastases Subgroups

Unfavorable Tumor Feature	Total % of Patients* (n = 1,675)	Age (months)				Pattern of Metastases			
		< 12 (n = 1,310)		12 to 18 (n = 365)		Stage 4S (n = 717)		Stage 4 (n = 958)	
		4S v 4 Pattern (%)	P	4S v 4 Pattern (%)	P	Age < 12 v 12 to 18 Months (%)	P	Age < 12 v 12 to 18 Months (%)	P
MYCN amplified	21	8 v 20	**< .001**	39 v 48	NS	8 v 39	**< .001**	20 v 48	**< .001**
Diploidy	27	21 v 28	**.0323**	32 v 41	NS	21 v 32	NS	28 v 41	**.0178**
11q aberration	20	10 v 21	NS	38 v 34	NS	10 v 38	**.06**	21 v 34	NS
1p aberration	27	16 v 30	**.0036**	50 v 46	NS	16 v 50	**.0032**	30 v 46	NS
Unfavorable histology	21	7 v 23	**< .001**	52 v 48	NS	7 v 52	**< .001**	23 v 48	**< .001**
Grade: undifferentiated	92	93 v 90	NS	91 v 92	NS	93 v 91	NS	90 v 92	NS
High MKI	16	4 v 17	**< .001**	50 v 43	NS	4 v 50	**< .001**	17 v 43	**< .001**
High LDH	57	44 v 63	**< .001**	67 v 72	NS	44 v 67	**.0059**	63 v 72	NS
Adrenal primary	64	73 v 56	**< .001**	43 v 66	**.0008**	73 v 43	**< .001**	56 v 66	**.0032**
Initial treatment: chemotherapy or other intensive	79	58 v 93	**< .001**	100 v 92	**.0476**	58 v 100	**< .001**	93 v 92	NS

NOTE. Bold font indicates significance.
Abbreviations: LDH, lactate dehydrogenase; MKI, mitosis-karyorrhexis index; NS, not significant ($P > .05$).
*No. of unknown patients excluded when calculating percentages with given characteristic.

multivariable Cox model testing more than two variables, *MYCN*, 11q, MKI, ploidy, and LDH were independently predictive of EFS (Appendix Table A6, online only).

A survival tree regression model identified *MYCN* amplification as the most highly prognostic factor, more so than age or metastatic pattern (Fig 3). Among patients with *MYCN* amplified tumors, MKI and then metastatic pattern (in low/intermediate MKI patients) were the most statistically significant predictors of outcome. Among those with *MYCN* nonamplified tumors, 11q was the most highly significant predictor of outcome. Among patients with 11q aberration, histology was significant, and in patients with normal 11q, 1p was significant. Of the 18 patients age 12 to 18 months with 4S pattern and *MYCN* nonamplified, normal 11q tumors, 5-year EFS and OS were 87.4% ± 10.3% and 100.0%, justifying their inclusion as very low risk in the INRG.

DISCUSSION

In this study, we have demonstrated that overall outcome for patients with neuroblastoma and stage 4S pattern is superior to that for patients with stage 4 pattern, and outcome for older patients is in general worse than that for younger patients (with exception of patients < 19 days of age). Age and metastatic pattern are highly significant prognostic factors.[21,27] However, age serves as a surrogate for evolving tumor biology in growing children, so it is not surprising that tumor biology is shown here to be more important than metastatic pattern or age. In patients younger than 18 months old with metastases, *MYCN* gene amplification, 11q aberration, MKI, 1p aberration, histology, and metastatic pattern can be used to classify patients into subgroups that are statistically significantly different in terms of outcome. The reason that toddlers age 12 to 18 months have similar EFS regardless of metastatic pattern seems to be because of similar frequencies of unfavorable biologic features for stage 4 and 4S pattern in the toddler age group.

INSS stage 4S has been established as having superior outcome compared with historical results with INSS stage 4 disease in infants younger than 12 months of age.[3,4] However, *MYCN* gene amplification has been shown to be an extremely important prognostic factor in infants with metastatic neuroblastoma in multiple cooperative studies, for infants with both stage 4S[3,9] and stage 4 disease.[28-30] Infants with either stage 4 or 4s neuroblastoma and *MYCN* gene amplification have a 2-year EFS of less than 30% despite intensive therapy,[28,30] whereas those without *MYCN* amplification may have a 2-year survival of greater than 90% with minimal or no chemotherapy.[29,31] Because of the rarity of *MYCN* amplification in infants with 4S neuroblastoma (0% to 10%), it has been difficult to show without the help

Table 3. Bivariate Analysis of Risk Factors in Stage 4S Metastatic Pattern

Risk Factor (category of increased risk)	Sample Size	Hazard Ratio	95% CI	P
Age (12 to < 18 months)	717	2.3	1.5 to 3.5	< .001
Age	564	NS		.33
MYCN (amplified)		4.1	2.6 to 6.2	< .001
Age	85	NS		.30
11q (aberration)		5.0	1.6 to 15.7	.0052
Age	196	NS		.68
1p (LOH)		3.3	1.7 to 6.6	< .001
Age	305	2.8	1.3 to 6.5	.0127
Ploidy (diploid)		1.9	1.0 to 3.8	.05
Age	337	NS		.87
Histologic classification (unfavorable)		4.3	2.2 to 8.4	< .001
Age	296	2.4	1.2 to 5.0	.0139
Grade (differentiated)		NS		.77
Age	282	NS		.67
MKI (high)		2.9	1.2 to 7.1	.0163
Age	460	2.1	1.3 to 3.6	.0040
LDH (≥ 580 U/L)		2.4	1.6 to 3.6	< .001
Age	677	2.3	1.5 to 3.5	< .001
Adrenal primary site (Yes)		NS		.59
Age	545	2.1	1.3 to 3.3	.0029
Initial treatment (chemotherapy and intensive therapy)		1.7	1.1 to 2.6	.0161

Abbreviations: LDH, lactate dehydrogenase; LOH, loss of heterozygosity; MKI, mitosis-karyorrhexis index; NS, not shown because not statistically significant.

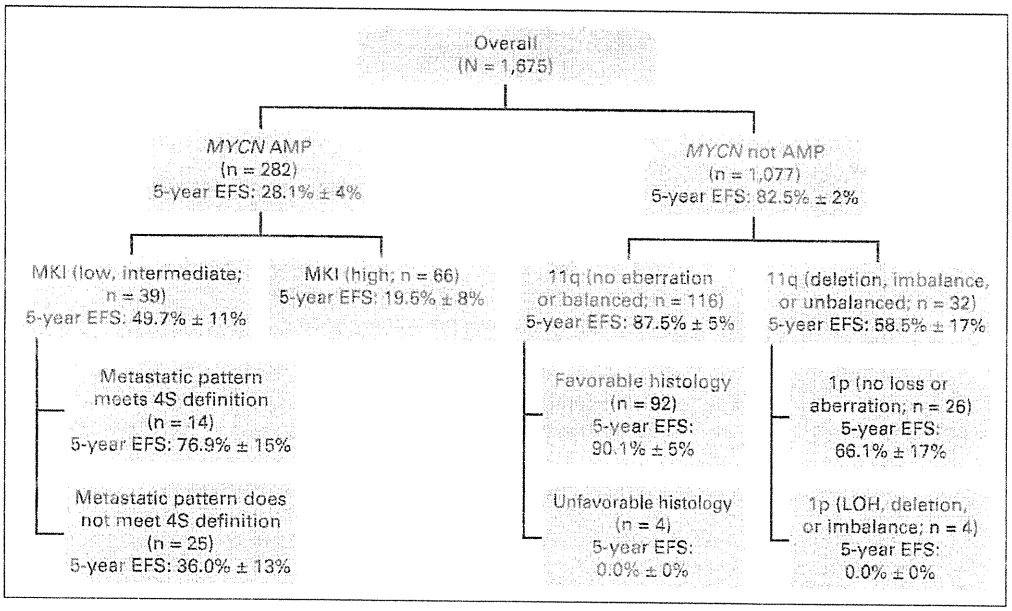

Fig 3. Survival tree regression analysis of patients with neuroblastoma younger than 18 months of age with metastatic disease (n = 1,675; event-free survival [EFS] ± SE). AMP, amplified; LOH, loss of heterozygosity; MKI, mitosis-karyorrhexis index.

of a large series such as the INRG database that *MYCN* status is prognostic independent of age and other factors. The favorable outcome for patients with stage 4 pattern without *MYCN* amplification was also extended to toddlers age 12 to 18 months. Two cooperative group analyses showed that this subgroup had a significantly superior survival to older patients with stage 4 disease as well as to those of the same age with *MYCN* gene amplification.[15,16] These findings prompted the revised INRG age limit for 4S metastatic pattern now designated Ms.[17]

In addition to *MYCN*, the other independently prognostic factors were 11q, MKI, ploidy, and LDH, despite the fact that a number of patients lacked information on these biologic variables. Within particular subsets in the survival tree, metastatic pattern, histology, and 1p were also significant. Attiyeh et al[32] reported 11q and 1p aberrations as independent unfavorable risk factors in a study of 915 patients, regardless of clinical risk classification. This study included nine of 50 patients with stage 4S and 11q aberration, although this small group was not analyzed separately. Spitz et al[33] compared 11q aberration in localized and 4S disease and found metastatic relapse rates to be 30% when 11q aberration was present and 3% with normal 11q status. Although a relatively low proportion of patients in our INRG series had assessment of 11q aberration (181 of 1,675 patients age < 18 months with metastases), the effect of 11q was so strong that even in this small sample, we found significance in multivariable analysis. Patients younger than 12 months or 12 to 18 months of age with *MYCN* amplified or 11q LOH tumors would not be considered low-risk patients and would warrant more intensive therapy despite the 4S pattern. Excluding such patients, there were only 18 patients who were age 12 to 18 months with *MYCN* not amplified and normal 11q tumors, with 5-year EFS and OS of 87.4 ± 10.3% and 100.0%, respectively.

Previous analyses of 4S disease have found unfavorable histology to be associated with decreased survival.[4,9] Diploid tumors have also been associated with poorer outcomes, but the prognostic benefits of hyperdiploid tumors seem to be limited to infants and toddlers age 12 to 18 months without *MYCN* amplification.[15] Elevated serum LDH may indicate increased tumor burden and has been identified as an independent poor prognostic factor.[3,9]

In our evaluation of infants with stage 4S disease, we found that risk of an event was high for patients of very young age, that the age subgroup with the best outcome was approximately 19 to 38 days, and that risk of an event increased gradually after age 38 days. Although the definition of young age varies by study, multiple groups have reported that infants younger than 2 to 3 months old have poorer OS than older infants.[3,4,9] Massive hepatomegaly in these infants can lead to respiratory, renal, and gastrointestinal impairment as well as coagulation abnormalities.[3] In the analysis by Nickerson et al[4] of 80 infants with 4S disease, five of the six recorded deaths occurred in infants younger than 2 months of age who had rapidly progressive abdominal disease. A literature review of 119 4S cases found that in 33 deaths, 11 of 12 deaths resulting from hepatomegaly occurred in infants diagnosed in the first 4 weeks of life.[13] These young infants with liver enlargement often are treated early and are at greater risk of death, thus explaining the observation in our INRG study that initial treatment is an unfavorable prognostic factor, as noted by others.[3]

Although this analysis used the largest cohort of patients with 4S metastatic pattern younger than 18 months of age, missing data and the rarity of some of the biologic tumor features resulted in some limitations. For example, some of the contributing groups at certain times allowed patients with so-called 4S disease younger than 12 months with tumors that crossed the midline as well as bone marrow involvement of more than 10%, characteristics that would have excluded patients from 4S categorization by the INSS definition; less than 10% bone marrow involvement was not required for any patient in the 12- to 18-month-old group with 4S pattern, because these patients were not defined as INSS 4S. It is unknown whether the size and stage of primary tumor are important in assigning 4S designation, but our study has shown that the pattern of metastases is less critical for risk group definitions than biologic variables. The most recent European infant protocols have used the metastatic pattern excluding macroscopic bone metastases but ignoring the primary tumor size as criteria for minimizing therapy in infants with metastatic neuroblastoma.[29] Finally, a variety of different treatment regimens were used, and thus, we were unable to adjust for treatment effect on EFS and OS. Acquisition of more complete data on biologic tumor features will be

